MODIS Ocean Science Team
Algorithm Theoretical Basis Document

ATBD 19

Case 2 Chlorophyll *a*

Version 7
30 January 2003

Kendall L. Carder, F. Robert Chen, Zhongping Lee, Steve K. Hawes, and Jennifer P. Cannizzaro

College of Marine Science
University of South Florida
140 Seventh Avenue South
St. Petersburg, Florida 33701
kcarder@monty.marine.usf.edu

TABLE OF CONTENTS

1.0 Introduction

The Case 2 chlorophyll a algorithm is based on a semi-analytical, bio-optical model of remote-sensing reflectance, $R_{rs}(\lambda)$, where $R_{rs}(\lambda)$ is defined as the water-leaving radiance, $L_w(\lambda)$, divided by the downwelling irradiance just above the sea surface, $E_d(\lambda,0^+)$.   The $R_{rs}(\lambda)$ model (Section 3) has two free variables, the absorption coefficient due to phytoplankton at 675 nm, $a_\varphi(675)$, and the absorption coefficient due to colored dissolved organic matter (CDOM) or gelbstoff at 400 nm, $a_g(400)$. The R_{rs} model has several parameters that are fixed or can be specified based on the region and season of the MODIS scene. These control the spectral shapes of the optical constituents of the model. $R_{rs}(\lambda_i)$ values from the MODIS data processing system are placed into the model, the model is inverted, and $a_\varphi(675)$, $a_g(400)$ (MOD24), and chlorophyll a (MOD21, Chlor_a_3) are computed.

The algorithm also outputs both the total absorption coefficients, $a(\lambda_i)$ (MOD36), and permits calculation of the phytoplankton absorption coefficients, $a_\varphi(\lambda_i)$ (MOD36), based on $a_\varphi(675)$ retrievals. These are used in the calculation of the absorbed radiation by phytoplankton (MOD22) for use in the calculation of chlorophyll fluorescence efficiencies (MOD20). MOD22 is also dependent upon the instantaneous photosynthetically available radiation (MOD22), which is discussed in ATBD20.

Algorithm development is initially focused on tropical, subtropical, and summer temperate environments, and the model is parameterized in Section 4 for three different bio-optical domains: (1) high ratios of photoprotective pigments to chlorophyll and low self-shading, which for brevity, we designate as "unpackaged"; (2) low ratios and high self-shading, which we designate as "packaged"; and (3) a transitional or global-average type. These domains can be identified from space by comparing sea-surface temperature to nitrogen-depletion temperatures for each domain (Section 5). Algorithm errors of more than 45% are reduced to errors of less than 30% with this approach, with the greatest effect occurring at the eastern and polar boundaries of the basins [*Carder et al.,* 1999]. Section 6 provides an expansion of bio-optical domains into high-latitude waters. The "fully packaged" pigment domain is introduced in this section along with a revised strategy for implementing these variable packaging domains. Algorithm errors are reduced from 41% for an empirical algorithm to 20% using the semi-analytical approach for global MODIS data in Section 7 [*Carder et al.,* 2003].

2.0 Overview and Background Information

According to the optical classification by *Morel and Prieur* [1977], oceanic waters may be characterized as Case 1, in which the optical properties are dominated by chlorophyll and covarying detrital pigments, or as Case 2, in which other substances, which do not covary with chlorophyll, also affect the optical properties. Such substances include gelbstoff, suspended sediments, coccolithophores, detritus, and bacteria. Pigment retrievals from Coastal Zone Color Scanner (CZCS) data in Case 1 waters

have achieved reasonable results (" 40% for local best cases [*Gordon et al.*, 1983]). However, substances not covarying with chlorophyll in Case 2 waters have caused the retrieval of pigment concentrations to have inaccuracies as high as 133% [*Carder et al.*, 1991].

CDOM absorbs light in an exponentially decreasing manner as a function of wavelength. Pheopigments, detritus, and bacteria similarly absorb more strongly at 412 nm than they do at 443 nm. Phytoplankton, on the other hand, absorb more strongly at 443 nm than at 412 nm. Thus, by measuring the relative amounts of light leaving the sea surface at those two wavelengths, we can estimate the relative amounts of phytoplankton and the other absorbing products mentioned above.

Winter convective over turn of the upper ocean layer also mixes up gelbstoff-rich deeper waters that have not been photo bleached unlike summer surface waters. These waters appear in CZCS data as being more chlorophyll-rich than measurements and models indicate [*Siegel and Michaels*, 1996].

The remote sensing reflectance, R_{rs}, model used to develop the algorithm presented here has a few parameters that cannot be fixed and applied to the entire globe; that is, they are site- and season-specific. This is due to the inherent variability of many bio-optical constituents. For example, absorption at 440 nm per unit chlorophyll *a* by phytoplankton can change with species and with nutrient and lighting conditions by more than an order of magnitude [*Morel and Bricaud*, 1981; *Kirk*, 1983; *Carder et al.*, 1991; *Morel et al.*, 1993; *Bricaud et al.*, 1995]. In addition, particle size and concentration have significant effects on the spectral backscattering coefficient $b_b(\lambda)$ of ocean water: pure water backscatter varies as - λ^{-4}, large-particle backscatter varies as - λ^{-0}, and backscatter by smaller-diameter detritus and bacteria varies with a spectral dependence between the two extremes [*Morel and Ahn*, 1990, 1991].

Many of these factors covary, allowing the simple wavelength-ratio algorithms of the CZCS [*Gordon and Morel*, 1983] to work fairly well. We have tried to understand many of these individual covariances and have developed empirical expressions for several individual bio-optical variables. By analyzing individual components of the model, we can gain a deeper understanding of the processes affecting the color of water-leaving radiance.

To the extent that such covariances change with season or bio-optical domains [e.g., see *Prieur and Sathyendranath*, 1981; *Sathyendranath et al.*, 1989; *Mitchell and Holm-Hansen*, 1991], we must consider temporal and spatial changes in algorithm parameterization. A strategy for partitioning the ocean into at least three different bio-optical domains on the basis of nutrient-temperature relationships, each with different model parameters, is discussed in Section 5. Section 6 provides an expansion of bio-optical domains from mainly tropical, subtopical, and summer temperate environments into high-latitude waters.

2.1 Experimental Objective

The main data product is chlorophyll *a* concentration, [chl *a*], which can be used as an indicator of plankton biomass, as an input to primary production models (MOD27), or to trace oceanographic currents, jets, and plumes. Other output products are $a_\varphi(675)$, $a_g(400)$, $a_\varphi(\lambda_i)$, and $a(\lambda_i)$. Total absorption, $a(\lambda_i)$, is necessary for calculating the light absorbed with depth for heat budget models. $a_\varphi(\lambda_i)$ is used in the IPAR/ARP MODIS algorithm (MOD22). $a_g(400)$ by itself can be used to map river plumes, to determine diffuse attenuation at that wavelength, or to calculate dissolved organic carbon (DOC) standing stocks and fluxes. In order to calculate DOC, we need to know how DOC concentration is related to DOC absorption. As coastal, estuarine, and other Case 2 environments become increasingly recognized as important areas of study, algorithms that can deal with the complex bio-optical properties of these regions will become available.

2.2 Historical Perspective

CZCS algorithms for estimating [chl *a*] plus pheophytin *a* concentrations perform quite well for regions of the ocean where scattering and absorbing components of seawater covary with these pigments, i.e., in Case 1 waters [*Gordon and Morel*, 1983; *Gordon et al.*, 1983]. A number of empirical and semi-analytical optical models have been developed to simulate the behavior of the underwater light field for such waters [*Morel and Prieur,* 1977; *Baker and Smith,* 1982; *Gordon et al.,* 1988; *Morel*, 1988; *Mitchell and Holm-Hansen*, 1991, *O'Reilly et al.,* 1998]. Such models have been used as the basis for classifying water types and/or for developing remote sensing algorithms.

However, the accuracies of these models decrease when environmental conditions depart from those representative of the data set used to empirically derive the covariance relationships. For instance, CDOM is produced when grazing, photolysis, and other mechanisms degrade the viable plant matter at and downstream from phytoplankton blooms. The CDOM-to-chlorophyll ratio will change dramatically for a parcel of upwelled water over a relatively short time, from chlorophyll-rich and CDOM-poor during a bloom to CDOM-rich and chlorophyll-poor after being grazed down. Solid evidence for the occurrence of this scenario can be found in two separate studies. *Peacock et al.,* [1988] found that absorption attributed to CDOM at 440 nm was at least 16 fold that due to phytoplankton pigments within an offshore jet from an upwelling region, whereas pigments were the dominant absorption agents at the upwelling center near the coast. Similarly, *Carder et al.,* [1989] found that particulate absorption at 440 nm decreased 13 fold while CDOM absorption at 440 nm increased by 60% in ten days for a phytoplankton bloom tracked from the Mississippi River plume to Cape San Blas. This widely varying CDOM-to-chlorophyll ratio has a profound effect on upwelled radiance in the blue 443 nm band of the CZCS, and a smaller but still significant effect in the green 520 nm band. For CDOM-rich waters, the correspondence

in absorption at 443 nm and 520 nm between CDOM and chlorophyll creates erroneously high estimates of pigment concentration in those models which rely solely upon either of these spectral bands to indicate absorption due to phytoplankton.

Carder et al., (1991) proposed that a short wavelength channel at around 410 nm could be used to distinguish CDOM (and other degradation products) from chlorophyll. Data for a channel at 412 nm is available not only for MODIS, but also for Ocean Color and Temperature Scanner (OCTS) and Sea-Viewing-Wide-Field-Sensor (SeaWiFS) imagery.

2.3 Instrument Characteristics

The algorithm requires input of the water-leaving radiance, L_w, at the MODIS ocean wave bands centered at 412, 443, 488, and 551 nm, respectively, and bio-optical domains are designated based upon sea-surface temperature (Section 5), a derived product of MODIS. R_{rs} is derived from the water-leaving radiance L_w [*Gordon and Wang*, 1994], as $R_{rs} = L_w(F_0 \cos \theta\ t_d)^{-1}$, where F_0 is the extraterrestrial solar irradiance, θ is the solar zenith angle, and t_d is the transmittance of light across the air-sea interface. The 1000 m resolution, new spectral bands, and near-daily coverage of MODIS will allow the observation of mesoscale oceanographic features in coastal and estuarine environments, areas seen to be increasingly important in many marine science studies in addition to traditional open-ocean observations.

3.0 Algorithm Description

Morel and Gordon [1980] describe three approaches to interpret ocean color data in terms of the in situ optical constituents: empirical, semi-empirical, and analytical. In the analytical approach, radiative transfer theory provides a relationship between upwelling irradiance or radiance and the in situ inherent optical properties backscattering and absorption [e.g., *Sathyendranath and Platt*, 1997]. Then, constituent concentrations are derived from irradiance or radiance values measured at several wavelengths by inversion of the resultant system of equations. The MODIS algorithm uses this approach, with the term "semi-analytical" invoked because bio-optical pieces of the radiative model are expressed by empirical relationships. The algorithms developed herein have been peer-reviewed and appear in condensed form in *Carder et al.,* [1999] and *Carder et al.,* [2002].

3.1 Theoretical Description
3.1.1 Physics of Problem

After light enters the ocean, some of it eventually scatters back up through the surface. This light is called the water-leaving radiance $L_w(\lambda)$, and it can be deduced from space after removal of atmospheric effects. The magnitude, spectral variation, and angular distribution of this radiance depend on the

following factors: the absorption and backscattering coefficients of the seawater, $a(\lambda)$ and $b_b(\lambda)$, respectively (known as the inherent optical properties); the downwelling irradiance incident on the sea surface $E_d(\lambda,0^+)$; and the angular distribution of the light within the ocean. To make things easier, we divide seawater into three components, each one having distinct optical properties of its own. These components are the seawater itself (water and salts), the particle fraction, and the dissolved fraction. Fortunately, $a(\lambda)$ is simply equal to the sum of the absorption coefficients for each component, and $b_b(\lambda)$ is equal to the sum of the backscattering coefficients. If we can accurately describe or model each spectrally distinct component of the absorption and backscattering coefficients, then we can determine the magnitude of each one from measurements of $L_w(\lambda)$ and $E_d(0^+,\lambda)$, given some assumptions about the angular distribution of light in the water. The key here is to accurately model the spectral behavior of $a(\lambda)$ for each component. The spectral behavior of $b_b(\lambda)$ is not as dynamic.

3.1.2 Mathematical Description of Algorithm

3.1.2.1 R_{rs} Model

The R_{rs} model is given by the following general equation, which is adapted from *Lee et al.,* [1994]:

$$R_{rs}(\lambda) = \frac{f\,t^2}{Q(\lambda)\,n^2} \frac{b_b(\lambda)}{[a(\lambda)+b_b(\lambda)]} \tag{1}$$

where f is an empirical factor averaging about 0.32–0.33 [*Gordon et al.,* 1975; *Morel and Prieur,* 1977; *Jerome et al.,* 1988; *Kirk*, 1991], t is the transmittance of the air-sea interface, $Q(\lambda)$ is the upwelling irradiance-to-radiance ratio $E_u(\lambda)/L_u(\lambda)$, and n is the real part of the index of refraction of seawater. By making three approximations, Eq. 1 can be greatly simplified.

1) In general, f is a function of the solar zenith angle, θ_0 [*Kirk*, 1984; *Jerome et al.,* 1988; *Morel and Gentili,* 1991]. However, *Morel and Gentili* [1993] have shown that the ratio f/Q is relatively independent of θ_0 for sun and satellite viewing angles expected for the MODIS orbit. They estimate that f/Q = 0.0936, 0.0944, 0.0929, and 0.0881, (standard deviation " 0.005), for λ = 440, 500, 565, and 665 nm, respectively. Also, *Gordon et al.,* [1988] estimates that f/Q = 0.0949, at least for θ_0 $ 20E. Thus, we assume that f/Q is independent of λ and θ_0 for all MODIS wavebands of interest, except perhaps for the band centered at 667 nm, which we don't use.

2) t^2/n^2 is approximately equal to 0.54, and although it can change with sea-state (Austin, 1974), it is relatively independent of wavelength.

3) Many studies have confirmed that $b_b(\lambda)$ is usually much smaller than $a(\lambda)$ and can thus be safely removed from the denominator of Eq. 1 [*Morel and Prieur*, 1977; references cited in *Gordon and Morel*, 1983], except for highly turbid waters.

These three approximations lead to a simplified version of Eq. 1,

$$R_{rs}(\lambda) \approx constant \frac{b_b(\lambda)}{a(\lambda)} \tag{2}$$

where the "constant" is unchanging with respect to λ and θ_0. The value of the constant is not relevant to the algorithm since, as will be shown later, the algorithm uses spectral ratios of $R_{rs}(\lambda)$ and the constant term factors out.

In the following sections, both $b_b(\lambda)$ and $a(\lambda)$ will be divided into several separate terms. Each term will be described empirically. The equations are written in a general fashion — i.e., the empirically derived parameters that describe each term are written as variables — and the actual values of the parameters that are used in the algorithm are shown in Tables 1a and 1b.

3.1.2.2 Backscattering Term

The total backscattering coefficient, $b_b(\lambda)$, can be expanded as

$$b_b(\lambda) = b_{bw}(\lambda) + b_{bp}(\lambda) \tag{3}$$

where the subscripts "w" and "p" refer to water and particles, respectively. $b_{bw}(\lambda)$ is constant and well known [*Smith and Baker*, 1981]. $b_{bp}(\lambda)$ is modeled as

$$b_{bp}(\lambda) = X\left[\frac{551}{\lambda}\right]^Y \tag{4}$$

The magnitude of particle backscattering is indicated by X, which is equal to $b_{bp}(551)$, while Y describes the spectral shape of the particle backscattering.

Lee et al., [1994] empirically determined X and Y values by model inversion using a formula similar to (4). The X and Y values were compared to the $R_{rs}(\lambda)$ values measured at each station with the purpose of finding empirical relationships for both X and Y as a function of $R_{rs}(\lambda)$ at one or more of the MODIS wavelengths. Once this was done, X and Y could be estimated from MODIS data. These empirical relationships are described below.

3.1.2.2.1 Expression for X

The general expression for X is

$$X = X_0 + X_1 \, R_{rs}(551) \tag{5}$$

where X_0 and X_1 are empirically derived constants. Linear regression performed on the derived values of X vs. $R_{rs}(551)$ taken from four cruises to the Gulf of Mexico (CP92, Tambax 2, GOMEX, and COLOR) resulted in X_0 and X_1 values of −0.00182 and 2.058 (n = 53, r^2 = 0.96). Figure 1 shows the regression graphically. If X is determined to be negative from Eq. 5 it is set to zero.
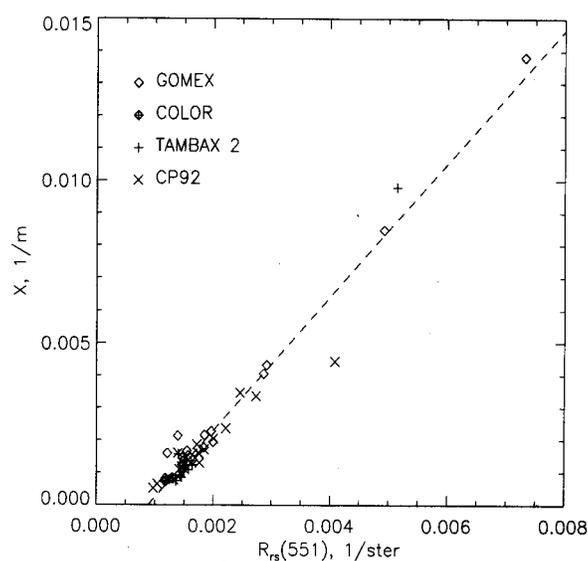
Figure 1. X versus $R_{rs}(551)$, where X is the magnitude of particle backscattering and R_{rs} is the remote sensing reflectance at 551nm. The line is the linear regression equation X=-0.00182 + 2.058 $R_{rs}(551)$ (n=53, r^2=0.96).

The values of X_0 and X_1 that are used in this version of the Case 2 chlorophyll algorithm are probably adequate for most of the globe and they are listed in Table 1. For regions influenced by river outflows, these parameters should be determined on a site-specific basis.

3.1.2.2.2 Expression for Y

Y was found to covary in a rather general way with the ratio $R_{rs}(443)/R_{rs}(488)$. Variations in numerator and denominator values of this ratio are largely determined by absorption due to phytoplankton

and CDOM. Absorption due to water is about the same and low at both wavelengths. Thus, to the extent that phytoplankton and CDOM absorption covary, the spectral ratio of the absorption coefficients, a(443)/a(488), will be only weakly dependent on pigment concentration, and the spectral ratio of backscattering coefficients should have a significant effect on the spectral ratio of R_{rs}. Y is thus represented as

$$Y = Y_0 + Y_1 \, \frac{R_{rs}(443)}{R_{rs}(488)} \qquad\qquad (6)$$

a linear function of $R_{rs}(443)/R_{rs}(488)$ where Y_0 and Y_1 are empirically derived constants.

Accurate measurements of $a_g(\lambda)$ and accurate removal of reflected skylight from the R_{rs} measurements are critical in determining Y by model inversion. Only data from the GOMEX and COLOR cruises are used here because the $a_g(\lambda)$ values were determined with a long-path spectrophotometer [*Peacock et al.,* 1994]. Linear regression of Y versus $R_{rs}(443)/R_{rs}(488)$ for stations from these two cruises resulted in Y_0 and Y_1 values of -1.13 and 2.57 (n = 22, $r^2 = 0.59$). Figure 2 shows the regression graphically. If Y is determined to be negative from Eq. 6 it is set to zero. A number of other spectral ratios of $R_{rs}(\lambda)$ were tested, but the 443:488 ratio had the highest correlation with Y.
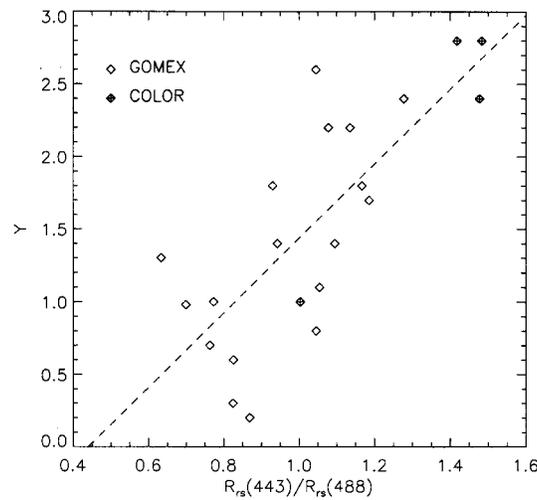
Figure 2. Spectral shape of particle backscattering Y versus $R_{rs}(443)/R_{rs}(488)$. The line is the linear regression Y = -1.13 + 2.57 $R_{rs}(443)/R_{rs}(488)$ (n=22, r^2=0.59).

The Y parameter should be large when the backscattering is due to small particles and/or water and vice versa [*Gordon and Morel*, 1983]. In oligotrophic regions we have determined values of Y greater than 2, while in waters with [chl *a*] > 10 mg m^{-3} the estimated Y values are often . 0. Where

gelbstoff concentrations are high, nutrients are typically high, and pigments are more packaged. Larger particles and lower Y values are expected to occur here, even with a lack of covariation between pigment and gelbstoff absorption.

3.1.2.3 Absorption Term

The total absorption coefficient can be expanded as

$$a(\lambda) = a_w(\lambda) + a_\phi(\lambda) + a_d(\lambda) + a_g(\lambda) \tag{7}$$

where the subscripts "w", "φ," "d," and "g" refer to water, phytoplankton, detritus, and CDOM ("g" stands for gelbstoff). Here $a_w(\lambda)$ is taken from *Pope and Fry,* [1997]. Expressions for $a_\phi(\lambda)$, $a_d(\lambda)$, and $a_g(\lambda)$ need to be developed.

### 3.1.2.3.1 Expression for a_ϕ

The shape of the $a_\phi(\lambda)$ spectrum for a given water mass will change due to the pigment-package effect (i.e., the flattening of absorption peaks due to self-shading with increasing intracellular pigment concentration and larger cell size) [*Morel and Bricaud,* 1981] and changes in pigment composition. For a given domain, normalizing measured $a_\phi(\lambda)$ curves to $a_\phi(675)$ reduces the dynamic range and results in a smooth variation for $a_\phi(\lambda)/a_\phi(675)$ vs. $a_\phi(675)$ for the MODIS wavebands centered at $\lambda = 412$, 443, 488, and 551 nm (see Figure 3) data for two high-light, subtropical regimes. To the extent that [chl *a*] is proportional to $a_\phi(675)$ (e.g. see Figure 4), Figure 3 demonstrates how the chlorophyll-specific absorption changes with chlorophyll concentration.

A hyperbolic tangent function was chosen to model this relationship in order to ensure that the value of $a_\phi(\lambda)/a_\phi(675)$ approaches an asymptote at very high or very low values of $a_\phi(675)$. *Carder et al.,* [1991] detail the behavior of this function with parameterization, although we have substituted $a_\phi(675)$ for the [Chl *a*] found in their expression. Using logarithmic scaling for both axes results in the following model equation for $a_\phi(\lambda)$ as a function of $a_\phi(675)$,

$$a_\phi(\lambda) = a_0(\lambda) \exp\left[a_1(\lambda) \tanh\left[a_2(\lambda) \ln\left(a_\phi(675)/a_3(\lambda) \right) \right] \right] * a_\phi(675) \tag{8}$$

where the parameters $a_0(\lambda)$ to $a_3(\lambda)$ are empirically determined for each MODIS wavelength of interest. $a_0(\lambda)$ is the most important of these parameters, as it is directly proportional to $a_\phi(\lambda)$. For simplicity, only $a_0(\lambda)$ and $a_1(\lambda)$ are varied to parameterize $a_\phi(\lambda)$, with $a_2(\lambda)$ and $a_3(\lambda)$ being set to the constant values of

−0.5 and 0.0112, respectively. Figure 3 shows the measured data and the modeled curves for $a_\varphi(\lambda)$ measurements taken from the GOMEX, COLOR, and TN048 cruises all considered to be part of the same high-light, subtropical domain (TN048 was an expedition to the Arabian Sea during monsoon conditions). The parameters $a_0(\lambda)$ to $a_3(\lambda)$ are listed in Table 1a.
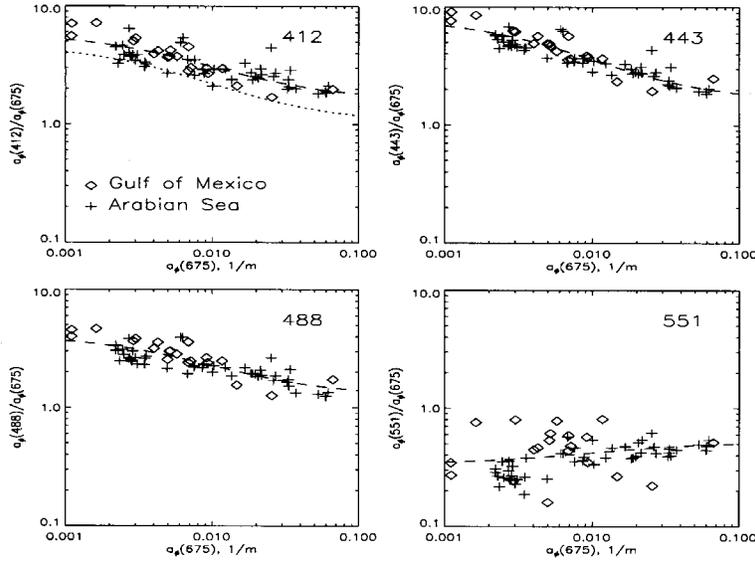
Figure 3. Absorption coefficients $a_\varphi(\lambda)/a_\varphi(675)$ versus $a_\varphi(675)$ for each Moderate-Resolution Imaging Spectrometer (MODIS) ocean wave band of interest. The number at top right corner indicates wavelength, λ. The lines are described by equation (8) using the parameters listed in Table 1a, and they represent the minimum sum-of-squares errors for modeled versus measured values of $a_\varphi(\lambda)/a_\varphi(675)$.

3.1.2.3.2 Expression for a_d and a_g

The $a_d(\lambda)$ and $a_g(\lambda)$ can both be fit to a curve of the form $a_x(\lambda) = a_x(400) \exp[-S_x(\lambda-400)]$ where the subscript "x" refers to either "d" or "g" [*Bricaud et al.,* 1981; *Roesler et al.,* 1989; *Carder et al.,* 1991]. Owing to this similarity in spectral shape, these terms cannot be spectrally separated with the MODIS channels, so the $a_d(\lambda)$ term is combined operationally with $a_g(\lambda)$, and both detrital and CDOM absorption are represented by $a_g(\lambda)$. The combined CDOM and detritus absorption term is thus written

$$a_g(\lambda) = a_g(400) \ \exp^{-S(\lambda-400)} \tag{9}$$

where S is empirically determined. Many researchers have reported that $S_d = 0.011$ nm^{-1}, on average [*Roesler et al.,* 1989]. For the GOMEX and COLOR cruises, an average value of 0.017 nm^{-1} was measured for S_g. Values reported by F. Hoge (personal communication) for the Sargasso Sea were

somewhat higher as are those found near swampy regions of the Gulf of Mexico. The algorithm performance was optimized by varying S_g, with the value 0.017 nm^{-1} providing the smallest residual error compared to field measurements (Table 1b). The increase in S is thought to account in part for the lack of gelbstoff fluorescene in the algorithm, which increases $L_w(412)$ [e.g. see *Mobley*, 1994].

As a final note on the R_{rs} model, Eqs. 5-9 are written in a general way to emphasize that the values of the parameters X_0, X_1, Y_0, Y_1, a_0, a_1, and S are not meant to be absolute. They should be updated and changed as more data become available. These parameters may also be changed with region and season to optimize algorithm performance.

3.1.2.4 Inverting the Model

All of the pieces of the reflectance model are now in place. Via Eqs. 2–4, and 5-9, $R_{rs}(\lambda)$ can be expressed solely as a function of the "constant" term, $R_{rs}(443)$, $R_{rs}(488)$, $R_{rs}(551)$, $a_\varphi(675)$, and $a_g(400)$, given values for the parameters for X_0, X_1, Y_0, Y_1, $a_0(\lambda)$, $a_1(\lambda)$, and S. $L_{wn}(\lambda)$ from MODIS can be converted into $R_{rs}(\lambda)$ as mentioned previously. Then, for each pixel, the R_{rs} model equation can be written for each of the 5 available MODIS wavebands yielding five equations written in three unknowns: the "constant" term, $a_\varphi(675)$, and $a_g(400)$.

Using spectral ratios of R_{rs} eliminates the "constant" term, since it is largely independent of wavelength. In principle, two spectral ratio equations can be used to solve for the two remaining unknowns, $a_\varphi(675)$ and $a_g(400)$. Based on the shape of the absorption curve for phytoplankton versus those for CDOM and detritus, equations using spectral ratios of 412:443 and 443:551 for $R_{rs}(\lambda)$ should provide a good separation of the two absorption contributions. Our two equations are

$$\frac{R_{rs}(412)}{R_{rs}(443)} = \frac{b_b(412)}{b_b(443)} \frac{a(443)}{a(412)}$$

$$(10)$$

$$\frac{R_{rs}(443)}{R_{rs}(551)} = \frac{b_b(443)}{b_b(551)} \frac{a(551)}{a(443)}$$

The right-hand side of each equation is a function of $a_\varphi(675)$, $a_g(400)$, $R_{rs}(443)$, $R_{rs}(488)$ and $R_{rs}(551)$. Since the R_{rs} values are provided on input, we now have two equations in two unknowns. The equations can usually be solved algebraically to provide values for $a_\varphi(675)$ and $a_g(400)$. The computational method of solving these equations is described in Section 3.2.

For waters with high concentrations of CDOM and chlorophyll, $L_w(412)$ and $L_w(443)$ values are small, and the semi-analytical algorithm cannot perform properly. It is thus designed to return values only when modeled $a_\varphi(675)$ is less than 0.03 m^{-1}, which is equivalent to [chl a] of about 1.5-2.0 mg m^{-3}. Otherwise, an empirical algorithm for [chl a] is used, which is described in Section 3.1.2.6.

3.1.2.5 Pigment Algorithm for Semi-analytical Case

When the semi-analytical algorithm returns a value for $a_\varphi(675)$, [chl a] is determined via a direct relationship to this value. This step requires knowledge of the chlorophyll-specific absorption coefficient for phytoplankton at 675 nm, $a_\varphi^*(675)$, for the bio-optical domain involved. *Bricaud et al.* [1995] demonstrated a wide range of values for $a_\varphi^*(675)$ using a global data set. If only surface values for waters in a more limited bio-optical domain (e.g., tropical and subtropical waters) are examined, however, this variability is greatly reduced. Phytoplankton found in high-light environments, for example, have relatively low concentrations of light-harvesting accessory pigments and relatively high concentrations of photoprotective pigments compared to plants found in samples from high latitudes, upwelling centers, or deep in the euphotic zone. Therefore the effects of accessory pigment absorption on the variability of the largely chlorophyll a dominated red peak at 675 nm are small in high-light environments. Furthermore, photoprotective pigments do not absorb light at 675 nm, and so they do not affect $a_\varphi(675)$, even if they are present in large quantities.

To evaluate variations of $a_\varphi(675)$ with [chl a] for subtropical to tropical waters, we developed a data set to explore the more limited variation in surface values of $a_\varphi^*(675)$ under high-light conditions (see section 4.2.1 for methodology). This data set came from surface-water samples from several cruises in the Gulf of Mexico (BONG 1, BONG 2, BOSS 1, and WFS) and one cruise to the Arabian Sea (TN048). Linear regression of log([chl a]) versus log[$a_\varphi(675)$] yielded an equation of the form

$$[chl\ a] = P_0 * [\ a_\phi(675)\ ]^{p_1} \tag{11}$$

For the data set mentioned above, the regression resulted in p_0 and p_1 values of 56.8 and 1.03, respectively ($n = 95$, $r^2 = 0.97$ on the log-transformed values). This regression and the data are shown in Figure 4. Within a given bio-optical domain, we find only a very weak change in $a_\varphi^*(675)$ with [chl a]. The exponent is close enough to 1.0 that little error occurs by linearizing the parameter values to 51.9 and 1.00, respectively, for that domain. This suggests an average $a_\varphi^*(675)$ value of 0.0193 m^2 (mg chl)$^{-1}$ for subtropical data sets**.**
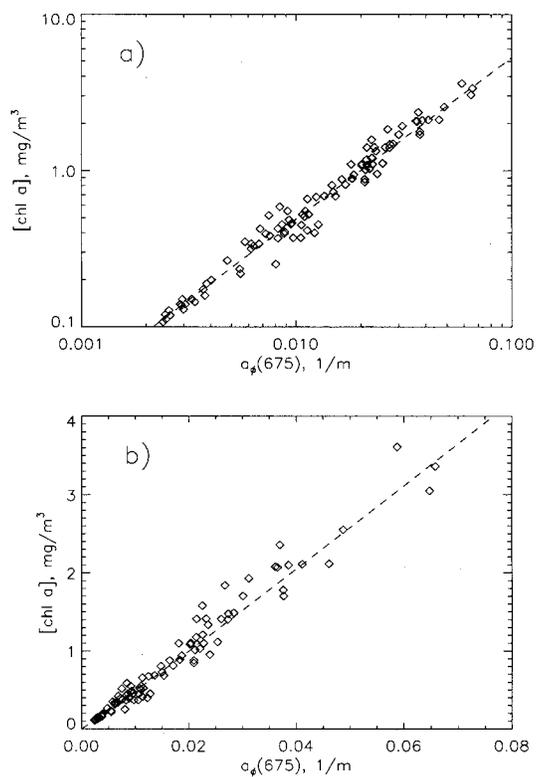
Figure 4. The [chl *a*] versus $a_\varphi(675)$ in (a) logarithmic scaling and (b) normal scaling. In both charts the dashed line is the equation [chl *a*] = 56.8 $[a_\phi(675)]^{1.03}$, which is the result of linear regression on the log-transformed values (n=96, r^2=0.97).

3.1.2.6 Pigment Algorithm for the Default Case

When the semi-analytical algorithm does not return a value for $a_\varphi(675)$, we provide an empirical, two-wavelength algorithm for [chl *a*] to use by default. *Aiken et al.,* [1995] found that the $L_w(488)/L_w(551)$ ratio is best for empirical [chl *a*] determination. We use an equation of the form

$$\log[chl\ a\ ]_{emp} = c_0 + c_1 \log(r_{35}) + c_2\,[\log(r_{35})]^2 + c_3\,[\log(r_{35})]^3 \tag{12}$$

where

$$r_{35} = \frac{R_{rs}(488)}{R_{rs}(551)} \tag{13}$$

[chl a]$_{emp}$ is called the "empirically-derived" or "default" chlorophyll a concentration, and c_0, c_1, c_2, and c_3 are empirically derived constants.

A subtropical and temperate summer data set was constructed from stations from the MLML 2, GOMEX, COLOR, TN042 and TN048 cruises, and from stations below 45 EN from the TT010 cruise (Table 2). This data set includes both open-ocean and riverine-influenced stations. A cubic regression of log([chl a]) against log(r_{35}) for measured [chl a] and $R_{rs}(\lambda)$ in this data set resulted in values of c_0 = 0.2818, c_1 = −2.783, c_2 = 1.863, and c_3 = -2.387. The data and the regression line are shown in Figure 5.
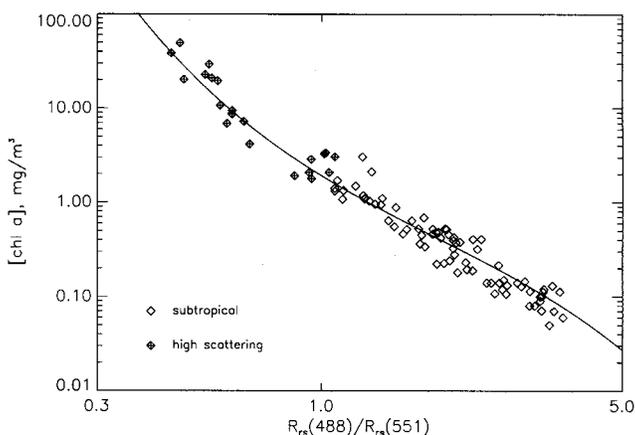
Figure 5. The [chl a] versus $R_{rs}(488)/R_{rs}(551)$ in log-log scaling. The dashed line represents a cubic regression on the log-transformed values and describes the default [chl a] algorithm.

3.1.2.7 Weighted Pigment Algorithm

Another consideration is that there should be a smooth transition in [chl a] values when the algorithm switches from the semi-analytical to the empirical method. This is achieved by using a weighted average of the [chl a] values returned by the two algorithms when near the transition border. When the semi-analytical algorithm returns an $a_\varphi(675)$ value between 0.015 and 0.03 m^{-1}, [chl a] is calculated as

$$[chl\ a] = w\ [chl\ a\ ]_{sa} + (1\ -\ w)[chl\ a\ ]_{emp} \tag{14}$$

where [chl a]$_{sa}$ is the semi-analytically-derived value and [chl a]$_{emp}$ is the empirically derived value, and the weighting factor is w = [0.03−$a_\varphi(675)$]/0.015.

3.1.2.8 Phytoplankton and CDOM Absorption Algorithms for Default Case

When the semi-analytical algorithm does not return a value for $a_\varphi(675)$, we provide empirical, multi-wavelength algorithms for $a_\varphi(675)$ and $a_g(400)$ based on $a_\varphi(440)$ and $a_g(440)$ [*Lee et al.,* 1998]. Using these results, the empirical, default algorithms for high $a_\varphi(675)$ values were determined by adjusting Lee's results to 675 nm for phytoplankton and to 400 nm for gelbstoff,

$$a_\phi(675)_{emp} = 0.328 * [10^{-0.919+1.037\rho_{25}-0.407\rho_{25}^2-3.531\rho_{35}+1.702\rho_{35}^2} - 0.008] \tag{15}$$

and for high $a_g(400)$ values,

$$a_g(400)_{emp} = 1.5 * [10^{-1.147-1.963\rho_{15}-1.01\rho_{15}^2+0.856\rho_{25}+1.702\rho_{25}^2}] \tag{16}$$

where ρ_{ij} are log of the ratio of the remote sensing reflectance of MODIS channel i to channel j.

Again, a weighted absorption algorithm similar to Equation 14 is used for each of these components to transition from the semi-analytical expression to the default expression.

The precision for the total absorption coefficients calculated empirically by *Lee et al.,* [1998] determined by the goodness of fit were 15.3 %, and for pigment absorption coefficients at 440 nm it was 29.1%. Transferring to 675 nm and considering global data sets will likely increase this uncertainty to perhaps 35% to 40%. The uncertainty of default $a_g(400)$ values is expected to be between 35% and 50%, although as with the semi-analytical values, there is a paucity of data sets to firm up these estimates.

3.1.2.9 Total and Phytoplankton Absorption Coefficients

The phytoplankton absorption coefficients $a_\varphi(\lambda_i)$ are calculated by inserting the modeled $a_\varphi(675)$ value into Eq. 8 and by using the necessary parameters from Table 1a for each wavelength. The total absorption coefficients $a(\lambda_i)$ are calculated by inserting the modeled $a_g(400)$ value and the *S* parameter from Table 1b into Eq.9 to get $a_g(\lambda_i)$ and then combining the result with the $a_\varphi(\lambda_i)$ and $a_w(\lambda_i)$ values using Eq. 7 and Table 1a.

3.2 Numerical computation

Here $a_\varphi(675)$ and $a_g(400)$ are determined from Eq. 10 with the substitutions discussed in section 3.1.2.4. Inverting one of the equations to isolate $a_g(400)$ and substituting into the other equation, all terms are then moved to one side. This yields a function that depends only on $a_\varphi(675)$ (given values for R_{rs} and

the algorithm parameters from Tables 1a and 1b). The value of $a_\varphi(675)$ at which the function crosses zero is the solution we seek. This solution is determined computationally via the bisection method. A 33-element array of $a_\varphi(675)$ values, scaled logarithmically from 0.0001 to 0.03 m^{-1} is created, and the function is evaluated at the two extremes. If the function changes sign between the two outermost values, a solution exists on the $a_\varphi(675)$ interval. The function is then evaluated at the midpoint of the array, and the half in which the function changes sign becomes the new search interval. In this manner the solution interval, which will be two adjacent points on the $a_\varphi(675)$ array, is determined in five iterations. Linear interpolation across the interval yields the semi-analytical $a_\varphi(675)$ value, and $a_g(400)$ is determined via either one of the ratio equations (Eq. 10) using the modeled value of $a_\varphi(675)$. If the function does not change sign across the two outermost values, a solution cannot be obtained and a switch is made to the empirical, two-wavelength, default algorithm.

When compared to an older method (look-up tables [*Carder et al.*, 1991]), the bisection method gave identical solutions to within five significant digits for $a_\varphi(675)$ and $a_g(400)$, and the code ran in 75% of the time required by the version of the code based on the look-up table.

The algorithm code is written in American National Standards Institute (ANSI) C. The program file contains about 300 lines of code and comments. It was developed and tested on a DEC Alpha machine. It was also tested on Silicon Graphics, SUN, and PC machines. All of the algorithm parameters listed in Tables 1a and 1b are read in from a file, so different parameter tables can easily be constructed for different applications (see below). The code is available upon request.

4.0 Algorithm Evaluation

4.1 Statistical criteria

To evaluate algorithm performance, we generated statistics that are determined on log-transformed variables so as to provide equal weight to data from all parts of the pigment and reflectance ranges. The slope and intercept values are from type II RMA regressions. The RMS statistic described is based on the root-mean-square of the logarithm of the ratio of modeled-to-measured values [*O'Reilly et al.*, 1998] and will be referred to here as RMS1. We also generated values for r^2 and root-mean-square error on the non-log-transformed (linear) data. This statistic will be referred to as RMS2 and is described by

$$RMS2 = \sqrt{\frac{\sum_{i=1}^{n}\left[\frac{x_{\mathrm{mod},i} - x_{obs,i}}{x_{obs,i}}\right]^2}{n-2}} \qquad (17)$$

where $x_{\text{mod},i}$ is the modeled value of the ith element, $x_{\text{obs},i}$ is the observed (or in situ or measured) value of the ith element, and n is the number of elements. Note that 10^{RMS1}-1.0 . RMS2 if there is no bias between the modeled and measured data. We used two graphical means of evaluating algorithm performance, scatterplots of modeled versus observed values and quantile-quantile plots [*O'Reilly et al.*, 1998].

4.2 Tests with University of South Florida Data

4.2.1 Methods

We initially tested our algorithm with our own subtropical and temperate-summer data set, called the Carder data set (Table 2), since observed values of $a_\varphi(675)$ and $a_g(400)$ are included wherever possible to accompany the observed $R_{rs}(\lambda)$ and [chl *a*] values. Also, 17 points from high-chlorophyll, high-scattering stations, mostly from the extended Mississippi River Plume region, are included. We later test the algorithm with global $R_{rs}(\lambda)$ and [chl *a*] data collected by international research teams and found in the NASA SeaBASS bio-optical data archive [*Hooker et al.,* 1994].

$R_{rs}(412)$, $R_{rs}(443)$, $R_{rs}(488)$, $R_{rs}(531)$, and $R_{rs}(551)$ for the Carder data set were derived from hyperspectral $R_{rs}(\lambda)$ measurements collected just above the sea surface (for measurement protocols, see *Lee et al.*, (1996)) by weighting to simulate the MODIS band responses [*Barnes et al.*, 1994]. Most $R_{rs}(\lambda)$ measurements in the SeaBASS global database were collected from just below the sea surface following the protocols of *Mueller and Austin* [1995]. Both data types are combined in algorithm performance tests against the global data.

All [chl *a*] values were determined fluorometrically [*Holm-Hansen and Riemann*, 1978; *Mueller and Austin*, 1995]. The $a_g(400)$ was determined by measuring the absorption of seawater filtered through a 0.2 μm pore-sized nylon filter in a spectrophotometer when compared to a MilliQ water blank [*Mueller and Austin*, 1995].

The method used to determine absorption coefficients for particles and for detritus involves filtering as much as 4 L of water through a 25 mm diameter, Whatman glass fiber filter (GFF). The protocols used are those discussed in *Mueller and Austin* [1995] and are based on methods developed by *Shibata* [1958], *Roesler et al.,* [1989], *Mitchell* [1990], *Nelson and Robertson* [1993], and *Moore et al.,* [1995]. In order to estimate absorption coefficients from the optical density, OD, measurements, an optical path-elongation factor, called β, which is dependent upon OD, is employed. Recently, however, it has been shown that β varies with the particle size prevalent to a region [*Moore et al.*, 1995]. This happens because smaller particles get more deeply embedded into the filter, providing a greater absorption cross section for photons scattered back and forth across the particle substrate than do the large particles remaining at the surface of the pad. For our work we chose a β factor appropriate for small,

subtropical particles that falls between two published β factors, one developed for detritus [*Nelson and Robertson*, 1993] and one for *Synechococcus* [*Moore et al.*, 1995]. Our β factor is

$$\beta = 1.0 + 0.6 \ OD^{-0.5} \tag{18}$$

Furthermore, we loaded the filter pads enough that the pad optical density exceeded 0.04 at 675 nm [*Bissett et al.*, 1997] for more accuracy in $a_\varphi(\lambda)$ measurements.

4.2.2 Results

The algorithm parameters used are shown in Tables 1a and 1b. [chl *a*], $a_\varphi(675)$, and $a_g(400)$ values were predicted by the semi-analytical algorithm with RMS1 errors of 0.122, 0.131, and 0.252, respectively, and with RMS2 errors of 0.289, 0.302, and 0.405, respectively (Table 4), for a largely subtropical or temperate-summer data set.

The results are also shown as scatter and quantile plots (Figure 6). The crosses on the plots are the points determined with the semi-analytical portion of the blended algorithm, and the diamonds represent points determined with the default or empirical algorithm. The high-chlorophyll points extend nicely along the one-to-one line on both the scatter and quantile plots. The RMS1 and RMS2 errors for [chl *a*] for this composite data set (*n*=104) were 0.132 and 0.300, respectively.

The [chl *a*] and $a_\varphi(675)$ data appear to be quite evenly clustered about the one-to-one line on both scatter and quantile plots with no aberrant tails at either end. The $a_g(400)$ points are predominantly below the one-to-one line and show a low bias. There are only 26 points in this plot because measured values of $a_g(400)$ are infrequently available for comparison. These data were subtropical except for some late-summer, temperate data, and they had relatively large specific absorption coefficients. Thus they are representative of the domain we designated as unpackaged.

4.3 Tests using a global data set

4.3.1 Data Set

A large (*n*=919) global evaluation data set consisting of measured R_{rs} values at the Sea-viewing Wide-field-of-view Sensor (SeaWiFS) wavelengths and chlorophyll *a* measurements based on both fluorometric and high-performance liquid chromatography (HPLC) methods was archived by the
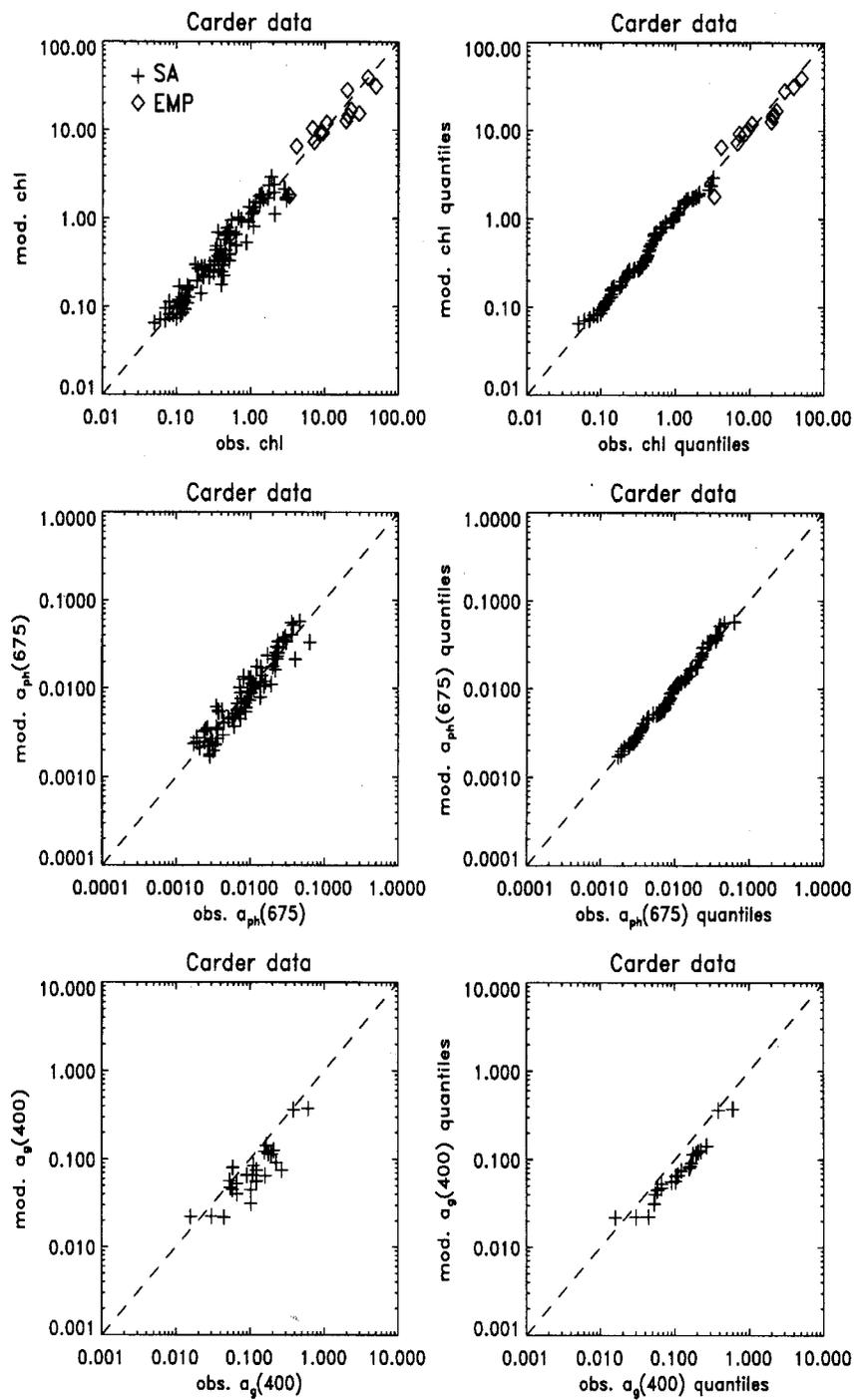
Figure 6. Algorithm performance for Carder data set, top observed versus modeled chl a, middle observed versus modeled $a_{ph}(675)$, and bottom observed versus modeled $a_g(400)$ in left scatterplots and right quantile-quantile plots. The lines are the one-to-one lines, SA (crosses) indicates points that are calculated semianalytically or by a blend of semianalytical and empirical values, while EMP (diamonds) indicates points that are calculated empirically.

NASA SeaWiFS Project as the SeaBAM data set [*O'Reilly et al.*, 1998]. These data came from various researchers around the United States and Europe and contain mostly subsurface R_{rs} values. In addition to these data, we have received 36 data points from the equatorial Pacific, consisting of R_{rs} measurements made above the surface (EqPac, courtesy of C. Davis), and we collected additional above-water data sets from the Southern California Bight (SCB) (April 1997 with G. Mitchell), near Hawaii (February 1997 with D. Clark), and the Kuroshio edge of the East China Sea (May 1997 with G. Gong), which we have added to the global data set. This combination of 976 data points allows for algorithm comparisons using a data set consisting of both above-water and below-water points.

The recent SCB data set provided an opportunity to compare above-water R_{rs} data with the historical California Cooperative Oceanic Fisheries Investigations (CalCoFI) SCB subsurface R_{rs} data set from the SCB. We also measured phytoplankton absorption spectra in the SCB in late winter to adjust $a_\varphi(\lambda)$ curve parameters, providing a more "packaged" parameterization (Table 3) for modeling the multiyear CalCOFI data set of subsurface R_{rs} values and similar eastern boundary environments.

4.3.2 Numerical Filters

Since many different locations and sensors were involved in compiling the SeaBASS data collections and as many as eight separate upwelling and downwelling sensor channels must be well calibrated to provide accurate spectral ratios of R_{rs} for the semi-analytical algorithm, an attempt was made to select an initial core set of data consistent with case 1 waters and with each other. Also, an attempt was made to partition the data sets into two regions, ones where little pigment packaging is to be expected (e.g., high-light, non-upwelling locations in warm, tropical and subtropical waters) and one where more packaging might be expected (e.g., eastern boundary upwelling, and non-summer high-latitude data). To assist in this task, each SeaBASS data set was individually examined.

Some of the data sets were composed of data largely falling into a single type of bio-optical domain according to the numerical filters discussed below. Others spanned two or more domains. Data sets falling primarily into the domain where the pigments appeared to be relatively unpackaged with significant photoprotective pigments [e.g., high $a_\varphi^*(443)$ and high $a_\varphi(443)/a_\varphi(675)$] were tested using the semi-analytical algorithm with the parameters shown in Tables 1a and 1b.

The first numerical filter compares the data sets to the historic [*Gordon et al.*, 1983] CZCS chlorophyll pigment algorithm [Chl $a = 1.14\,[r_{25}]^{-1.71}$, $r_{25} = R_{rs}(443)/R_{rs}(550)$] to check for consistency with this classical algorithm for case 1 waters with relatively little packaging. Figures 7d, 8d, and 9d show scatterplots of observed [chl a] versus r_{25} for different sets of warm-water data, with the CZCS algorithm illustrated by the dashed line. The warm-water, subtropical and tropical data sets, with little in the way of pigment packaging and probably high photoprotective to chlorophyll ratios (Figure 7d), were

found to be centered over the CZCS algorithm for pigment values less than about 1 mg m^{-3}.

When the CZCS algorithm was applied to data from high-latitude or eastern boundary upwelling locations where pigments are packaged into larger cells with more self-shading (Figure 8d), however, the CZCS-like chlorophyll a values were typically 50% to 90% lower than those measured. This effect of differing bio-optional domains on the performance of the CZCS-like algorithm suggests that regional algorithms are needed to obtain best results for different regions or seasons as suggested by *Mitchell and Holm-Hansen* [1991].

This "filter" approach helped us separate various data sets into two domains, which we call the unpackaged-pigment domain and packaged-pigment domain. This type of domain-selection filter, however, cannot be applied to satellite-derived data because of the need for measurements of [chl a]. Thus a second type of numerical filter was sought that was reliant on only space-derived data.

The second numerical filter uses the ratios $r_{12} = R_{rs}(412)/R_{rs}(443)$ and r_{25} (Figures 7b, 8b, and 9b) and is applicable to satellite-derived data. For the Carder data set the line $r_{12} = 0.95 \, [r_{25}]^{0.16}$ was used to separate high-gelbstoff data points (those below the line in Figure 7b) from the case 1 data. On the basis of the Carder a_g data, the gelbstoff-rich case 2 data had $a_g(400)$ values typically in excess of the relationship $0.12 \, [\text{chl } a]^{0.7}$ or $a_g(443) > a_\varphi(443)$. This line also separates case 1 data representative of more packaged domains from those representative of less packaged domains since the ratio r_{12} is less affected by packaging effects than is r_{25}. Thus, for waters far from terrigenous influences, the second filter provides a flag for packaging effects.

Case 1 waters with more packaged pigments from a traditional upwelling region (e.g., CalCOFI) were also examined using the second numerical filter. These data fell mostly below the filter line (Figure 8b) in comparison to the unpackaged data, which fell mostly above the line (Figure 7b). Since pigment packaging reduces the absorption for a given concentration of pigments far more at 443 than at 551 nm, and somewhat more at 443 than at 412 nm [*Morel and Bricaud*, 1981], packaging and reduction of photoprotective pigments significantly increases r_{25} while increasing the r_{12} ratio somewhat. This places packaged data points below the $r_{12} = 0.95 \, [r_{25}]^{0.16}$ line (Figure 8b) even without excessive gelbstoff concentrations, at least for points with r_{25} values in excess of a value of about 3.0. Filter 2, then, provides a space-based method for separating data points with packaged pigments from those with unpackaged pigments, at least for the oligotrophic end of the data sets.

Filter 2, however, can be distorted by a poorly calibrated sensor or by inaccurate atmospheric correction, so it is inadvisable to use it exclusively as a packaging filter without some means of providing an independent check on its performance. A means of accomplishing this task is found in Section 5.

4.4 Algorithm evaluation with the "unpackaged" data set

Those data sets generally found to be consistent with the CZCS algorithm line and which were located primarily above the line $r_{12} = 0.95 \, [r_{25}]^{0.16}$ for points where $r_{25} > 3.0$, were numerically classified as unpackaged, in reference to the pigment-absorption effects on the optics prevalent at those locations at the time of data collection. Those data sets with high-r_{25} points largely below the line were classified as packaged, and a test of a packaged algorithm is developed and discussed below. Those data sets with high-r_{25} points fairly equally divided by the line were withheld from the tests of both the unpackaged and packaged algorithm, but they were included as part of the test of a global algorithm developed and discussed below.

There are 287 data points in the unpackaged ensemble data set: 134 USF data points and 37 EqPac, equatorial Pacific points, all measured above water and processed using the *Lee et al.,* [1996] protocols, and an additional 126 EqPac points, all measured below the surface using the *Mueller and Austin* [1995] protocols. Of these points, 261 (91%) were processed by the semi-analytical portion of the [chl *a*] algorithm, yielding RMS1 and RMS2 errors of 0.099 and 0.230, respectively (Table 4). The scatter (Figure 7a) and quantile (Figure 7c) plots overlay the one-to-one line at the ends as well as in the middle. For the log-transformed variables, the type II RMA slope was 0.999, the bias was 0.002, and the correlation coefficient r^2 was 0.873. When all 287 data points were considered using the semi-analytical algorithm plus the blended and empirical algorithms, RMS1 and RMS2 errors were 0.108 and 0.242, respectively. The type II RMA slope was 0.973, the bias was -0.003, and r^2 was 0.955. Note that for this unpackaged data set, the transition from the semi-analytic to the default algorithm is reasonably smooth (Figure 7c).

Table 4 provides a complete summary of these statistics. Note that since these algorithms are largely semi-analytical in nature and were developed based mostly upon Gulf of Mexico data for the parameterization, one would not expect to have slope values of 1.000 and bias values of 0.000. Note also that the r^2 values increased using the blended algorithm because of the extended range of chlorophyll *a*. It is important to note that RMS2 errors of less than 25% significantly exceed our accuracy goal of 35% or less.

4.5 Algorithm evaluation with the "packaged" data set

Several data sets within the global evaluation set were numerically diagnosed as coming from waters where the pigments were much more packaged than those from the warm, tropical and subtropical data sets evaluated earlier. The new packaged parameters, shown in Table 3, are used to define a slightly different, packaged algorithm for upwelling and winter-spring temperate regions.

There are 326 points in an ensemble of multiyear, multiseason data sets from the California
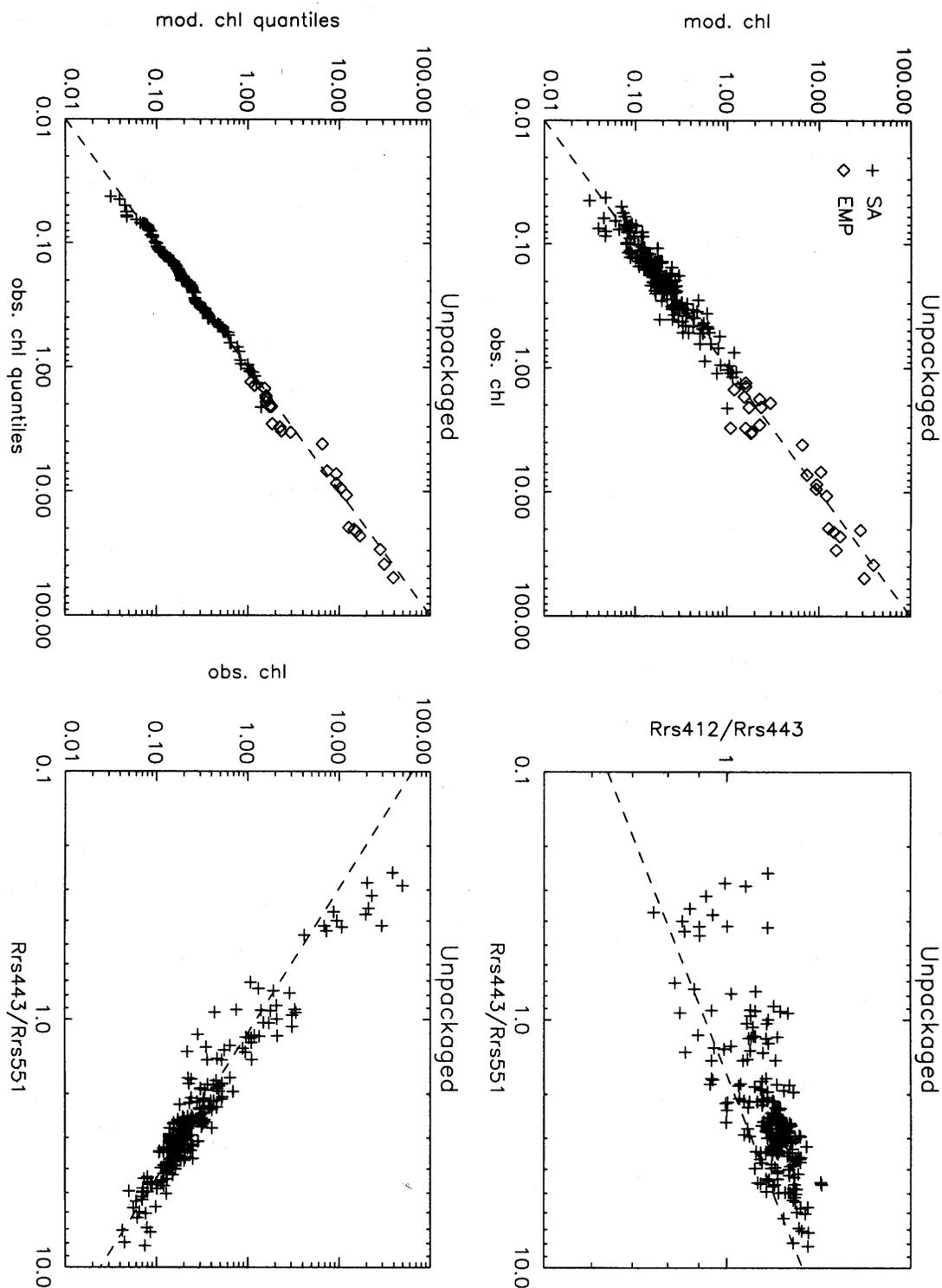
Figure 7. Algorithm performance for and analysis of data sets passing the "unpackaged" numerical filter. (a) Scatterplot of observed versus modeled chl a (mg m^{-3}). The dashed line is the one-to-one line. (b) The r_{12} versus r_{25}, with the line, $r_{12}=0.95[r_{25}]^{0.16}$, used to identify "unpackaged" case 1 data (above line). (c) Quantile-quantile plot of observed versus modeled chl a. (d) Observed chl a versus r_{25}, with the Coastal Zone Color Scanner (CZCS) algorithm line $C=1.14[r_{25}]^{-1.71}$.
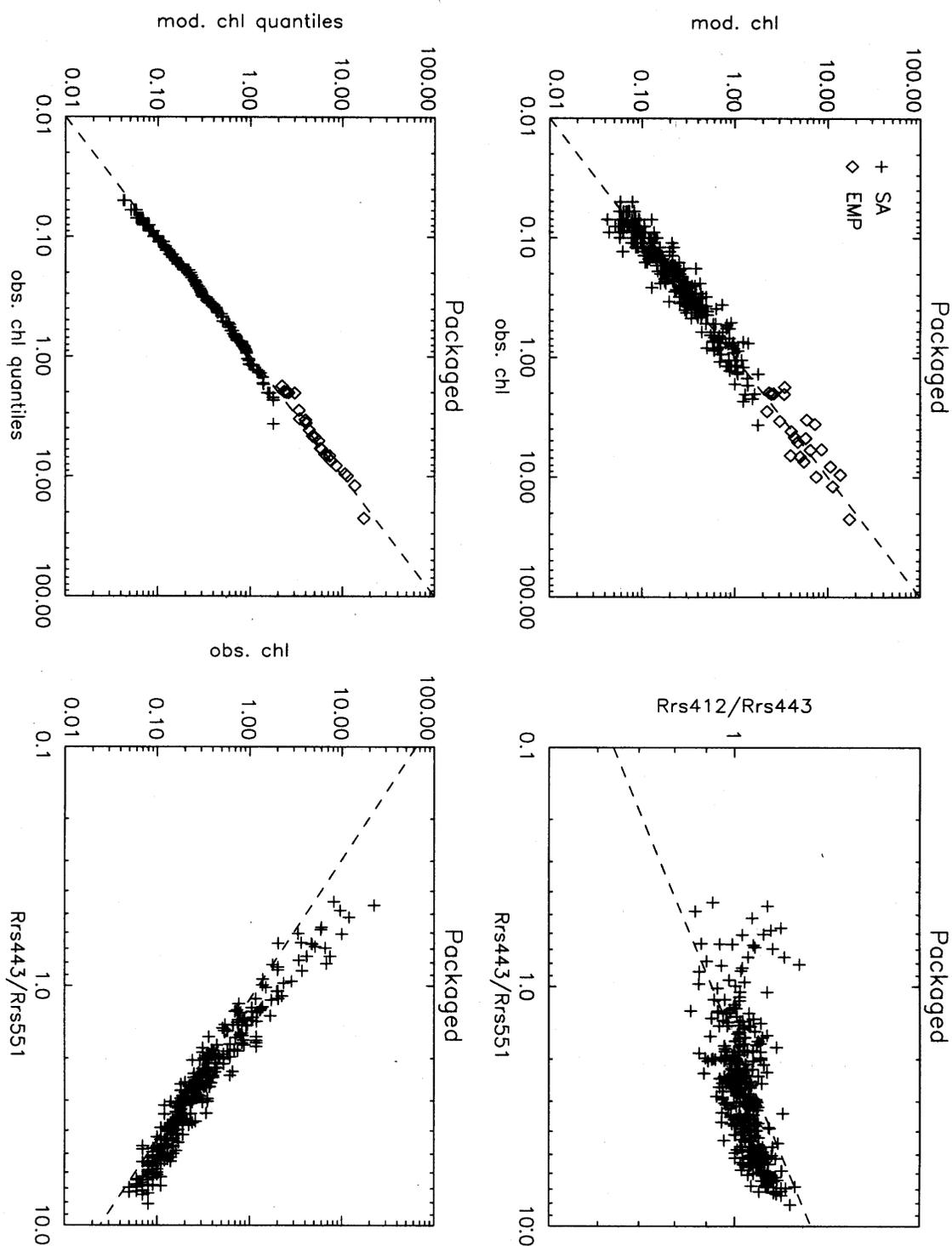
Figure 8. Algorithm performance for and analysis of data sets passing the "packaged" numerical filter. (a) Scatterplot of observed versus modeled chl a (mg m^{-3}). The dashed line is the one-to-one line. (b) The r_{12} versus r_{25}, with the line, $r_{12}=0.95[r_{25}]^{0.16}$, used to identify "packaged" data (below line). (c) Quantile-quantile plot of observed versus modeled chl a. (d) Observed chl a versus r_{25}, with the Coastal Zone Color Scanner (CZCS) algorithm line $C=1.14[r_{25}]^{-1.71}$.

Current which we label as packaged. These consist of historical CalCOFI (n=303) and recent Cal9704 (n=23) data which we recently collected with G. Mitchell. The CalCOFI R_{rs} data were subsurface measurements, while the Cal9704 data were above-surface collections. Three hundred and three points (93%) from this packaged data set passed the semi-analytical portion of the new algorithm, yielding RMS1 and RMS2 errors for [chl *a*] retrieval of 0.111 and 0.268, respectively. The type II RMA slope was 0.999, the bias was -0.006, and the r^2 value was 0.917. The scatterplot (Figure 8a) overlays the one-to-one line, and the quantile plot (Figure 8c) is linear and overlies the one-to-one line but has a slight discontinuity near a chlorophyll value of 3. This indicates that some parameter modifications for the packaged algorithm are needed in this transition region.

Using the blended algorithm on 326 data points, the r^2 increased to 0.951 while the other statistics remained about the same (Table 4). The RMS2 error of about 28% for the packaged algorithm also is better than our accuracy goal of 35% or less.

4.6 Algorithm evaluation with a global data set

To generate an algorithm to smoothly transition between regions and periods where there are packaged and unpackaged pigments, we developed a global data set combining the packaged, unpackaged, and other mixed data sets from the SeaBASS archive. This data set has 976 data points. We then developed a set of compromise parameters for this global-average algorithm, shown in Table 3, for use at times and places where packaging is unknown or transitional. For this data set and these average parameters, 883 (90.5%) of the points passed the semi-analytical portion of the algorithm, yielding RMS1 and RMS2 errors in algorithm-derived [chl *a*] of 0.176 and 0.446, respectively.   The type II RMA slope was 1.003, the bias was 0.002, and r^2 was 0.852. Statistics for the entire n=976 set were similar, except r^2 was higher (0.913) (Table 4).   The scatterplot (Figure 9a) looks evenly clustered about the one-to-one line, and the quantile plot (Figure 9c), though sinuous, overlays the one-to-one line for the most part. Again, the results from the semi-analytical algorithm fall below those for the default algorithm near the transition region. This can be alleviated by reducing the "blending" domain from $0.015 < a_{\varphi}(675) < 0.03$ to $0.008 < a_{\varphi}(675) < 0.015$.

If we are unable to accurately specify the packaging domains of the world ocean, such a compromise global algorithm with about 44% accuracy is likely to be the best accuracy that can be achieved. This does not meet our accuracy goal of 35% or better, so a focused effort is being made to develop an accurate sorting mechanism based on space-derived data to define the bio-optical domains of the ocean on a spatial and temporal basis.
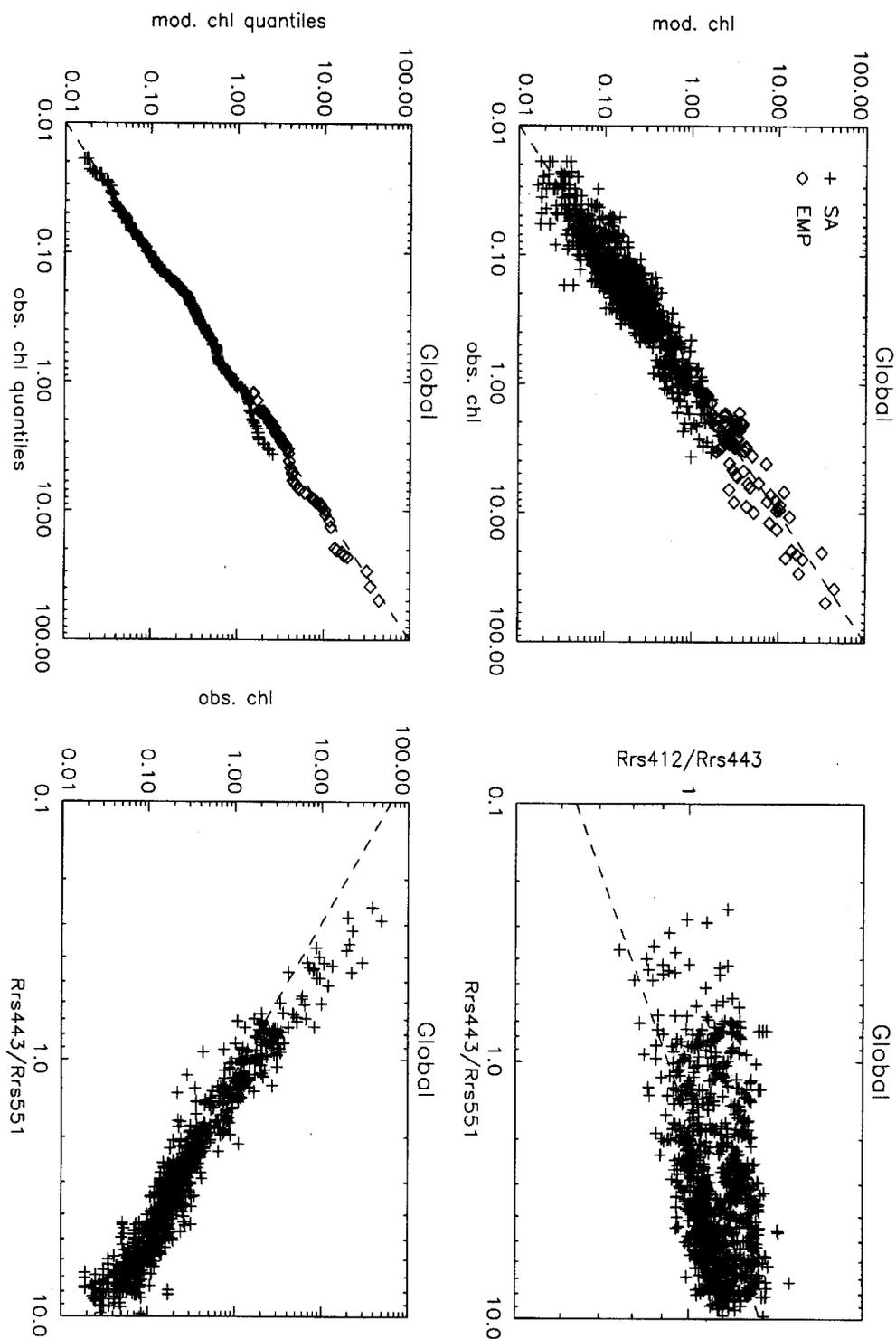
Figure 9. Algorithm performance for and analysis of global data sets without partitioning into "packaged" and "unpackaged" subsets. (a) Scatterplot of observed versus modeled chl a (mg m^{-3}). The dashed line is the one-to-one line. (b) The r_{12} versus r_{25}, with the line, $r_{12}=0.95[r_{25}]^{0.16}$. (c) Quantile-quantile plot of observed versus modeled chl a. (d) Observed chl a versus r_{25}, with the Coastal Zone Color Scanner (CZCS) algorithm line $C=1.14[r_{25}]^{-1.71}$.

**5.0 Strategy for Implementation of Variable Package Parameters**

5.1 Nitrate depletion temperatures

The biggest limitation to algorithm development for the global ocean is a paucity of bio-optical field data from around the globe that are complete with ancillary particle and gelbstoff absorption spectra and auxiliary data such as sea-surface temperature, salinity, and nutrients. These data are needed in order to assess the spatial and temporal variation in the key algorithm parameters: X, Y, S, and, most important, $a_0(\lambda)$ and $a_1(\lambda)$. In order to derive [chl a], it is vitally important to be able to predict how the $a_\phi(\lambda)$/[chl a] ratio varies. Thus we must study the effect of light history, which is related to season, cloudiness, and latitude, as well as nutrient history, which is influenced by mixed-layer depth, upwelling, river plumes, and offshore/onshore proximity.

While algorithms appropriate for regions with strictly packaged or unpackaged pigments can reduce the uncertainty in chlorophyll a concentration from perhaps 45-50% to less than 30%, methods based upon space-derived data that determine when and where to apply the appropriate parameterization are still under development. One method using space-derived data (numerical filter 2) has already been discussed, but it is only definitive for waters where $r_{25} > 3.0$. Also, stations with high gelbstoff concentrations can cause confusion using this method, and inaccurate atmospheric correction can cause confusion using this method on any given day. For offshore oligotrophic to mesotrophic waters, however, it is a very useful diagnostic tool if used under clear atmospheric conditions.

A second space-based approach uses the fact that unpackaged pigments are usually found in high-light, nutrient-poor waters where small-diameter phytoplankton cells predominate [e.g., *Herbland et al.*, 1985; *Carder et al.*, 1986]. Since dissolved nutrients cannot be detected from space, a nutrient surrogate was sought. *Kamykowski* [1987] developed a model that explained much of the covariance observed between upper layer temperatures and nitrate concentrations [e.g., *Kamykowski and Zentara*, 1986]. D. Kamykowski (personal communication, 1998) has since developed nitrate-depletion temperatures (NDTs) for the North Atlantic Ocean. The nitrate-depletion temperature is defined as that temperature at which nitrate could no longer be detected, at least using techniques of the era from about 1960-1985. These NDTs provide a means to observe from space a variable that indicates when and where nitrate may be limiting phytoplankton growth and where upper layer production is dependent upon recycled nitrogen. Such phytoplankton are typically small [*Herbland et al.*, 1985] with unpackaged pigments [*Carder et al.*, 1986].

To delimit regions of the North Atlantic Ocean that likely contain unpackaged pigments, we have compared sea-surface temperatures to Kamykowski's NDTs. Figure 10 shows annual trends in sea-surface temperature, CZCS pigment, and NDTs for the Gulf of Maine, Bermuda, and Barbados. The temperatures and pigments are 4-year (1982-85) monthly averages from the Advanced Very High
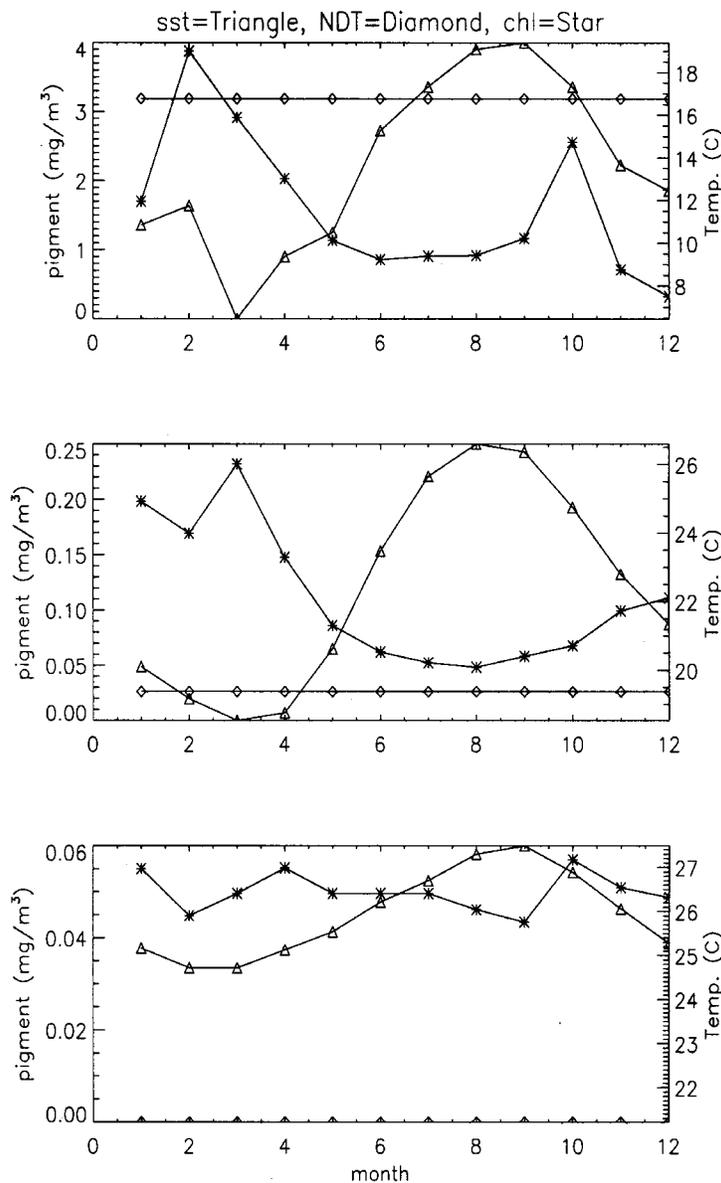
Figure 10. Four-year (1982-1985), monthly mean values of sea-surface temperature (triangles), CZCS pigment (astericks), and nitrate-depletion temperature (diamonds) for locations near (top) the Gulf of Maine, (middle) Bermuda, and (bottom) Barbados.

Resolution Radiometer (AVHRR) and CZCS sensors archived by the Jet Propulsion Laboratory, Physical Oceanography, satellite data archive (USA_NASA_JPL_PODAAC_A005). Note that based on this approach, waters in the Gulf of Maine are rarely designated as being nitrogen limited, and those near Barbados are always designated as being nitrogen limited, while those near Bermuda are designated as being limited in the summer and unlimited in the winter-spring. Clearly, the Gulf of Maine is a lower-light, higher-nutrient environment than are Bermuda and Barbados, so the degree of packaging there is

likely to be much higher.

By analyzing bio-optical data in the SeaBASS archive, some preliminary functional relationships between the NDTs and pigment-packaging classifications for the north Atlantic Ocean were empirically derived using sea-surface temperature (SST) derived from the AVHRR satellite sensor: (1) unpackaged domain: SST > NDT + 3.0^o C, (2) transitional or global domain: NDT +1.8^o C < SST < NDT + 3.0^o C, and (3) packaged domain: SST < NDT + 1.8^o C.

These domains for the months of February and August are shown for an El Niño year (1983) and a normal year (1985) in Plate 1, based upon climatological sea-surface temperatures. Here the tropics and most of the subtropics apparently contain phytoplankton with unpackaged pigments, except in the northwest African, Peruvian, and equatorial upwelling regions. Here transitional and packaged pigments can be observed during part of the year. High-latitude regions are mapped with this method as packaged, gradually transitioning toward the equator into the unpackaged domain again. Note the marked difference in the domains between El Niño and "normal" years, especially in the tropics and subtropics.

Using AVHRR SST data from the physical oceanographic data archive, bio-optical data from SeaBASS for a cruise crossing several domains were sorted by domain using NDTs. Data for the transition period from spring to summer from the NASA SeaBASS archive were sorted into the three bio-optical domains, and the appropriate algorithm parameterization was applied to derive chlorophyll *a* values. May Atlantic Meridional Transect (AMT 4) data along 20° W longitude, North Sea data and MLML2 data collected in July, and GOMEX1 and GOMEX2 data collected in April and June provide a diverse set of north Atlantic observations that were sorted by the NDT filter and processed. The results (Figure 11) are compared with those obtained by simple use of the global (transitional) algorithm. The RMS1 and RMS2 errors for this diverse data set were 0.153 and 38%, respectively, for domain-sorted data, while the errors grew to 0.186 and 50%, respectively, when all were processed using global or transitional parameters for the algorithm without sorting by domain.

Since the spring-summer transition and eastern basin, upwelling data are perhaps the least predictable in terms of pigment packaging, the error reduction observed of 12% is indicative of the improvements that can be made by sorting ocean color data into bio-optical domains before applying algorithms. A community-wide effort to evaluate and modify this approach for other regions is an on-going task.

5.2 Test of MODIS Algorithms with SeaWiFS Data

A major end-to-end test of all MODIS Ocean Team products was undertaken under the direction of Dr. Robert Evans at the University of Miami using prototype MODIS processing software. SeaWiFS
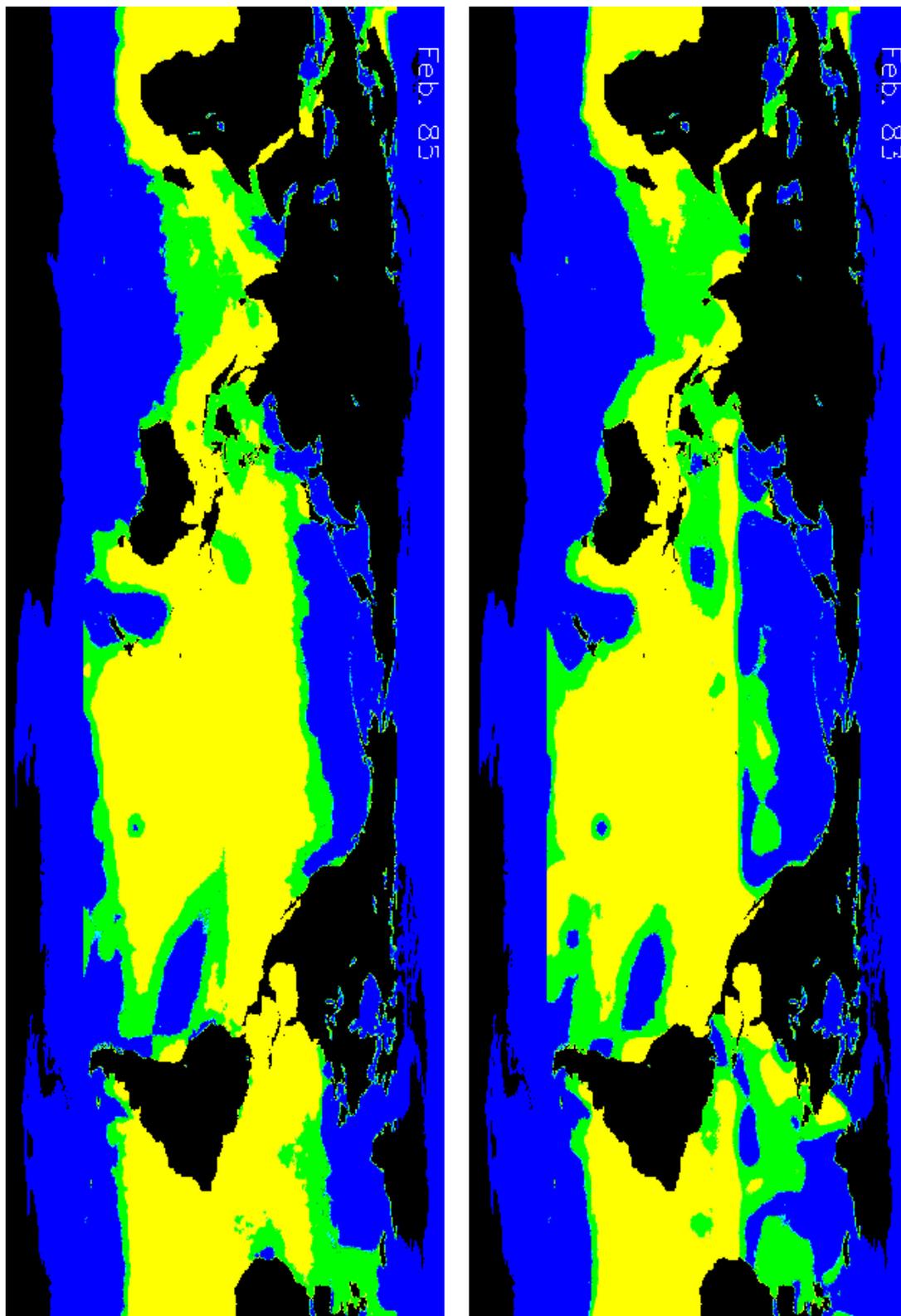
Plate 1. Bio-optical domains for the global ocean based on 1983 and 1985 monthly mean temperature compared to nitrate-depletion temperatures (NDTs) for (a) February and (b) August. Here black, blue, green, and yellow regions depict land, packaged, transitional, and unpackaged domains, respectively.
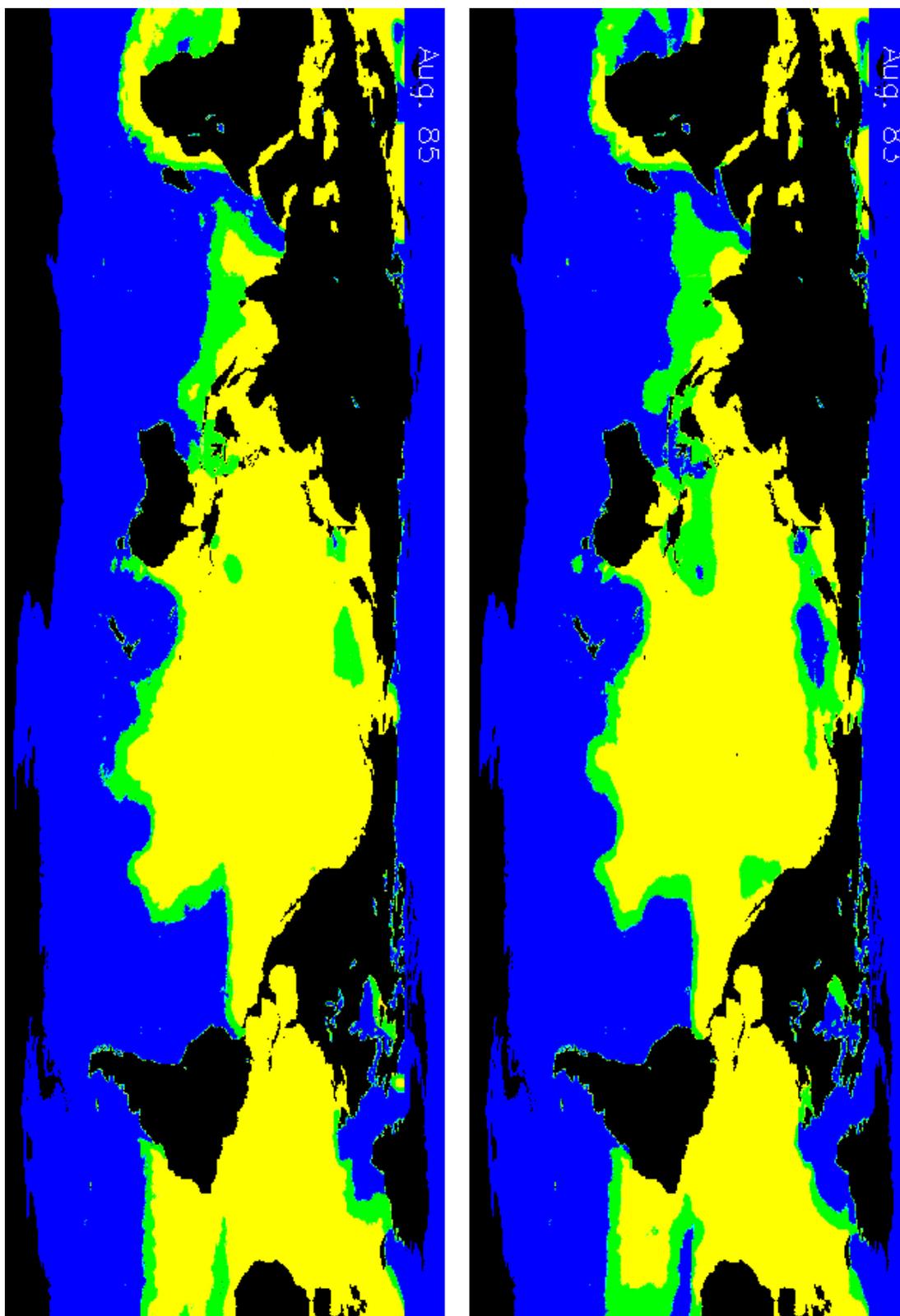
Plate 1. (Continued)
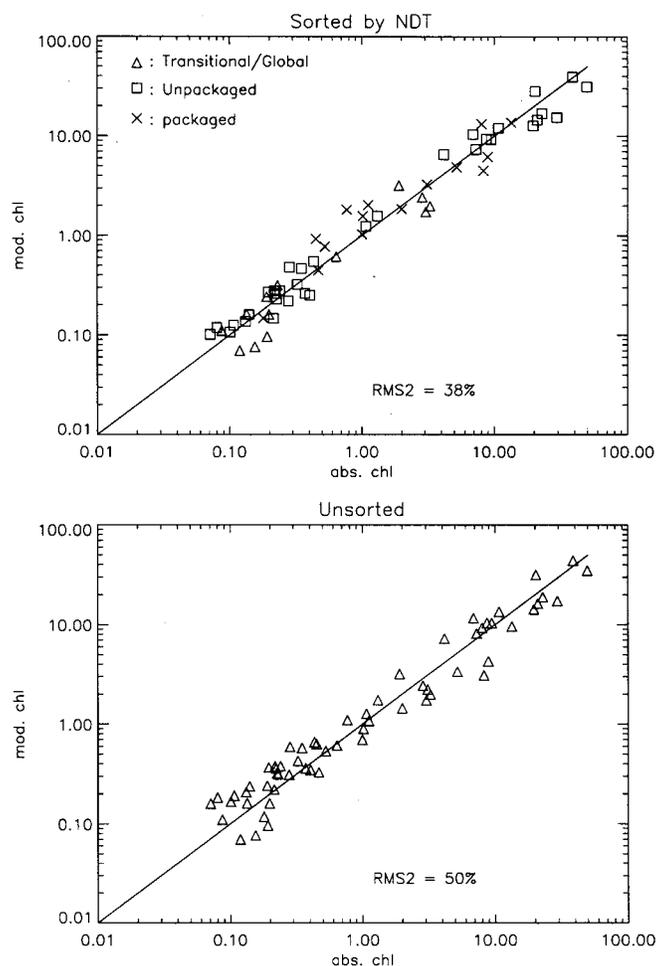
Figure 11. Comparisons of algorithm-derived and measured chlorophyll a values for (top) domain-sorted data for the North Atlantic Ocean during the spring-summer transitional period and (bottom) unsorted data.

data were modified to match Level 1 data from the MODIS data stream and processed. This processing included atmospheric correction and production of Level 2, 3, and 4 products [*Hawes et al.,* 2000]. All data products discussed under ATBD19 were successfully processed for a 2-day simulation of global data. These included $a_\varphi(675)$, $a_g(400)$, [chl *a*], a(412), a(443), a(490), a(532), and a(551). These products were successfully passed on for processing of absorbed radiation by phytoplankton (MOD22) and fluorescence efficiency (MOD20).

6.0 Expansion of bio-optical domains into high-latitude regions

The dominant effects of pigment packaging when transitioning from tropical to temperate waters are included in the original version of the semi-analytic chlorophyll algorithm described previously in

Section 3 and tested in Sections 4 and 5 [*Carder et al.,* 1999]. The "packaged" parameter set, however, which was derived from Southern California temperate data significantly underestimates chlorophyll concentrations when applied to high-latitude data.

Studies in the Southern Ocean indicate that chlorophyll-specific phytoplankton absorption coefficients are lower compared to Southern California waters due to increased pigment packaging and lower detrital absorption [*Sosik et al.,* 1992; *Reynolds et al.,* 2001]. Since phytoplankton absorption typically has the largest impact on remote-sensing reflectance ratios, such differences in $a_\varphi^*(\lambda)$ cause the relationship between oceanic reflectance ratios and chlorophyll *a* concentration in both Antarctic and Arctic waters [*Mitchell and Holm-Hansen,* 1991; *Mitchell,* 1992] to deviate from empirically derived relationships generated from mostly northern mid- and low-latitude data [e.g. *Gordon et al.,* 1983; *O'Reilly et al.,* 1998]. Indeed, the application of these latter two-band empirical algorithms to high-latitude CZCS and SeaWiFS imagery has consistently led to significant underestimations of chlorophyll concentration in the Southern Ocean [*Sullivan et al.,* 1993; *Moore et al.,* 1999] and the Bering Sea [*Maynard and Clark,* 1987; *Müller-Karger et al.,* 1990]. Furthermore, estimates of primary production derived from models based on satellite-derived chlorophyll fields may be significantly underestimated in polar regions as Antarctic and Arctic waters contribute 20% to global annual primary production [*Behrenfeld and Falkowski,* 1997].

Thus, the domain of "packaged" parameters, previously discussed in Section 4.5, is expanded in this section in order to reflect the inherent optical variability displayed in high-latitude polar waters. In addition, a smoother blending mechanism to transition between packaging domains is introduced that continues to be based on nitrate-depletion temperatures.

6.1 Development of the "fully packaged" parameter set

While the "unpackaged" parameter set remains the same as in Tables 1a and 1b, the "packaged" parameter set has been revised. This domain is now based on Antarctic, Arctic and temperate upwelling-center data and will be referred to as the "fully packaged" parameter set.

The shape of the $a_\varphi(\lambda)$ spectrum was modified for the fully packaged parameter set using data collected during spring from the Bering Sea (MF0796) and from the Antarctic Polar Frontal Zone (REV9802). Measurement locations, dates, and sources are listed in Table 5. The parameters $a_0(\lambda)$ to $a_3(\lambda)$ from Equation 8 were optimized to provide a minimum sum-of-squares error for modeled versus measured values of $a_\varphi(\lambda)/a_\varphi(675)$. Figure 12 shows the data and the modeled fully packaged curve for $a_\varphi(443)$ along with the unpackaged curve for comparison. All fully packaged algorithm parameters are listed in Table 6.
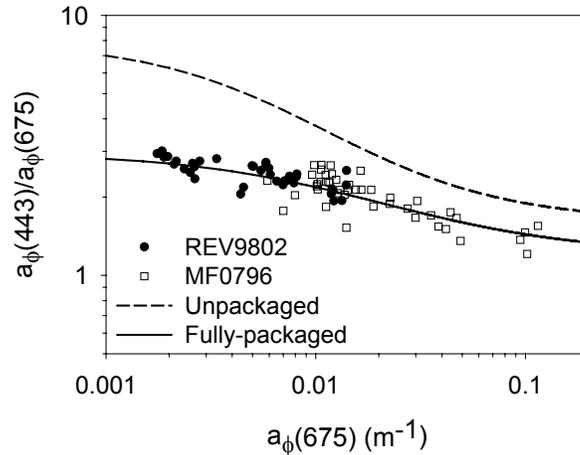
Figure 12. The ratio $a_\varphi(443)/a_\varphi(675)$ versus $a_\varphi(675)$ for high latitude data from the Bering Sea (MF0796) and the Antarctic Polar Frontal Zone (REV9802). The lines are described by equation 8 using the parameters listed in Table 1a and Table 6.

The relationship between $a_\varphi(675)$ and [chl *a*] was modified using Cal9704 upwelling-center data to reflect the lowest chlorophyll-specific absorption coefficients expected for phytoplankton cells from high-nutrient regions that are exposed to low-light levels. A p_0 coefficient of 79.4 in Equation 11 for fully packaged waters is equivalent to using an $a_\varphi^*(675)$ value of 0.0126 m^2 (mg chl)$^{-1}$, which is close to the lower limits determined in previous studies [*Bricaud et al.,* 1995; *Cleveland,* 1995].

The default empirical chlorophyll algorithm parameters, c_0 to c_3, were modified using Cal9704 and MF0796 data. Regression of $\log_{10}([chl\ a])$ against $\log_{10}(R_{rs}(488)/R_{rs}(551))$ for measured [chl *a*] and $R_{rs}(\lambda)$ in this data set resulted in values of $c_0=0.51$, $c_1=-2.34$, $c_2=-0.40$, and $c_3=0.00$ (n=35) using Equation 12, yielding RMS1 and RMS2 errors of 0.102 and 25%, respectively. Figure 13 shows the data and the modeled fully packaged curve along with other high-latitude empirical expressions from the Southern Ocean [*Arrigo et al,* 1998; *Dierssen and Smith,* 2000] and the Labrador Sea [*Cota et al.,* 2000].

The new "fully packaged" algorithm is very similar to the *Cota et al.* [2000] relationship for chlorophyll concentrations less than 5.0 mg m^{-3}. At chlorophyll concentrations greater than 5.0 mg m^{-3}, the relationship more closely resembles the *Dierssen and Smith,* [2000] line. The divergence of the *Arrigo et al.,* [1998] diatom and *Phaeocystis* line away from the Cryptophyte line suggests that at high chlorophyll concentrations, no single empirical expression will perform accurately in the Southern Ocean. This is due to regional [*Brody et al.,* 1992; *DiTullio and Smith,* 1996; *Goffart et al.,* 2000] and seasonal [*Moline et al.,* 1999] shifts in phytoplankton dominance together with the tendency of blooms dominated by a single class of phytoplankton to exhibit a large variability in $a_\varphi^*(\lambda)$.

The slope coefficient, S, for the combined CDOM and detrital absorption term (Equation 9) was

decreased for the fully packaged parameter set from 0.0225 to a value of 0.017. Applying this lower slope value with the Antarctic data optimized algorithm performance and is thought to account for the low chlorophyll-specific detrital [*Sosik et al.,* 1992; *Clementson et al.,* 2001] and CDOM [*Reynolds et al.,* 2001] coefficients observed in Antarctic waters and perhaps low photobleaching. Since Arctic waters exhibit higher diffuse attenuation coefficients for CDOM compared to Antarctic waters perhaps due to higher riverine input [*Mitchell,* 1992], we propose to continue using a slope coefficient of 0.0225 for Arctic fully-packaged data and only use a value of 0.017 for Antarctic fully packaged data.
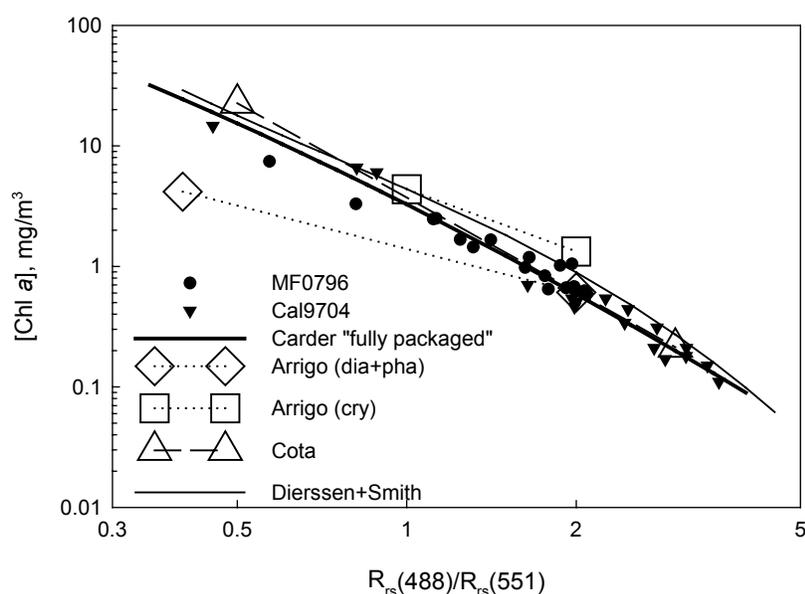
Figure 13. The [chl *a*] versus $R_{rs}(488)/R_{rs}(551)$ default empirical algorithm for the "fully packaged" pigment domain. The Carder "fully packaged" line (solid thick) represents a quadratic regression on log-tranformed Bering Sea (MF0796) and Southern California (Cal9704) data. Also shown are high-latitude algorithms from the Ross Sea [*Arrigo et al., 1998*] for regions dominated by diatoms (dia) and Phaeocystis (pha) and by cryptophytes (cry), from the region west of the Antarctic peninsula [*Dierssen and Smith, 2000*], and from the Labrador Sea [*Cota et al., 2000*]. Lines are plotted approximately for the original range of values only.

The wavelength independent parameters (i.e. X_0, X_1, Y_0, and Y_1) used in Equation 5 and 6 for determining the magnitude and shape of particulate backscattering in Equation 4 remain unchanged for the fully packaged parameter set. Although modeled [*Dierssen and Smith,* 2000] and measured [*Reynolds et al.,* 2001] results indicate that chlorophyll-specific particulate backscattering is lower in the Southern Ocean compared to northern mid- and low-latitude waters, Equation 5 corrects for this effect. Essentially, the lower green reflectance values ($R_{rs}(551)$) observed in high-latitude southern waters for a given chlorophyll concentration [*Reynolds et al.,* 2001] shall yield lower $b_{bp}(551)$ values using this equation.

6.2 Revised strategy for implementation of variable package parameters

      With the addition of the fully packaged parameter set, a new means for implementing the various packaging parameters within the semi-analytic algorithm is required. As the previous stair-stepping type of approach for transitioning between packaging domains based on nitrate-depletion temperature (discussed in Section 5.0) resulted in unrealistically, large chlorophyll variations in regions with sharp temperature changes (e.g. Florida Gulf Stream and upwelling regions) (data not shown), a smoother transition among the domains is needed.

      A blending mechanism identical to the one used to provide a smooth transition between the semi-analytic and empirical algorithm products (i.e [chl a], $a_\varphi(675)$, and $a_g(400)$) (discussed in Section 3.1.2.7) has been established by studying an intense upwelling environment off southern California. Most of the variability in pigment packaging was observed to be limited to a $5^{o}C$ range about the nitrate-depletion temperature (NDT). The most packaged pigments there resembled $a_\varphi^{*}(\lambda)$ spectra observed during April in the Bering Sea data (Figure 12). Thus, phytoplankton absorption parameters from low-light and nutrient-replete polar waters (fully packaged) and parameters from high-light and nutrient-poor tropical/ subtropical and summer temperate waters (unpackaged) are designated as end members. A linear blending algorithm provides for the transition between the two end members. The algorithm is run first using both the unpackaged and the fully packaged parameter sets where NDT - $1.0^{o}C$ < SST < NDT + $4^{o}C$. Chlorophyll concentration is then calculated as

$$[chla] = w[chla\,]_{UP} + (1 - w)[chla\,]_{FP} \qquad (19)$$

where [chl a]$_{UP}$ is the unpackaged value, [chl a]$_{FP}$ is the fully packaged value, and the weighting factor is w=[1.0 + (SST-NDT)]/5.0. For regions outside this transitional domain, the fully packaged parameter set is used where SST < NDT-$1.0^{o}C$ and the unpackaged parameter set is used where SST > NDT+$4.0^{o}C$. Thus, for any satellite location, the SST is compared to the NDT, and the level of pigment packaging is defined as either fully packaged, transitional, or unpackaged (Figure 14). The same approach is used to blend the unpackaged and fully packaged pigment domains for algorithm retrievals of $a_\varphi(675)$ and $a_g(400)$.

      Algorithm performance using the revised pigment packaging parameters together with the smoother blending strategy was first evaluated using the Cal9704 data set. Cold (~$12^{0}C$), nutrient-rich, and chlorophyll-rich waters upwelled off the coast of California in April 1997 (Figure 15), displayed low $a_\varphi(443)/a_\varphi(675)$ ratios consistent with low-light, shade-adapted phytoplankton populations observed during April in the Bering Sea. The data were sorted into the three bio-optical domains (fully packaged,

transitional, or unpackaged) based on SST's and NDT's using the new blending strategy, and the appropriate algorithm parameters were applied. The algorithm results are shown in Figure 16. The RMS1 and RMS2 errors were 0.116 and 31%, respectively, for domain-sorted chlorophyll data. The errors, however, increased to 0.148 and 39% for RMS1 and RMS2, respectively, when average packaging parameters were used (e.g. Eq. 19 with a weighting factor of 0.5). Sorting ocean color data into bio-optical domains, therefore, reduced the error by 8% and allowed the algorithm to meet the 35% accuracy goal originally proposed for this algorithm.
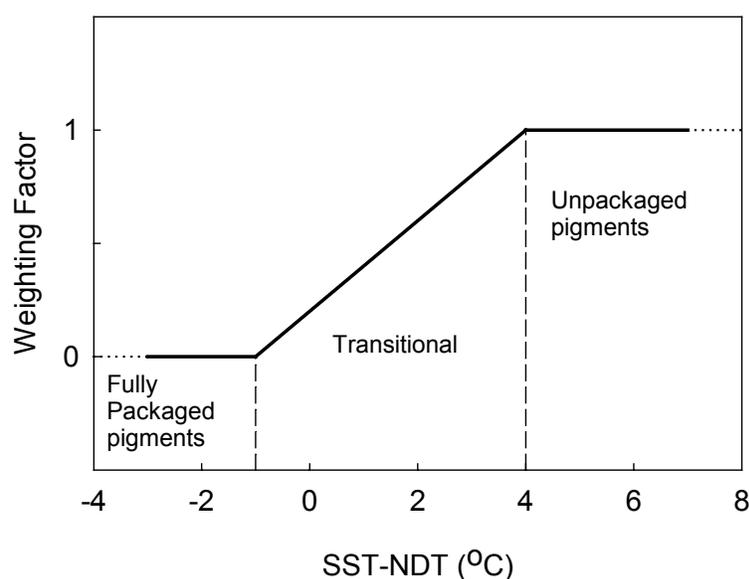
Figure 14. Blending mechanism for transitioning between unpackaged and fully packaged pigment domain based on the difference between the sea surface temperature (SST) and the nitrate depletion temperature (NDT). The weighting factor used in Equation 19 for SST-NDT < -1.0°C is zero, for -1.0°C < SST-NDT < 4.0°C is between zero and one, and for SST-NDT > 4.0°C is one.

6.3 Algorithm evaluation of a high-latitude data set

6.3.1 Data set

A large multi-region, multi-season, and multi-investigator high-latitude data set (n=871) has been compiled that includes Antarctic data extracted from the NASA SeaBASS data archive, spring Bering Sea data (MF0796), and Arctic data kindly provided by G.Cota (ODU) (Table 5). This data set which includes $R_{rs}(\lambda)$ and fluorometrically determined chlorophyll concentrations is used to test the revised packaging parameters along with the new transitioning strategy based on nitrate-depletion temperatures. Although a small subset of this data was used to derive the fully packaged parameter set being tested here, the only $R_{rs}(\lambda)$ data used was to determine the default empirical chlorophyll algorithm (Figure 13). Since the
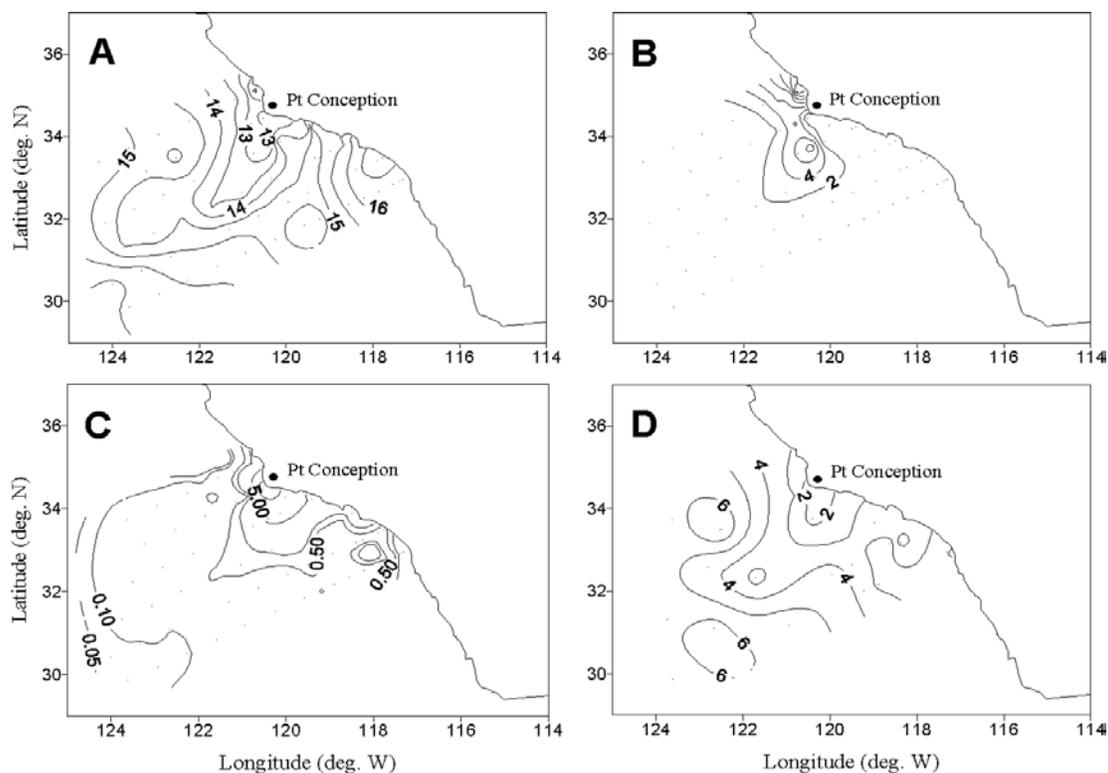
Figure 15. Surface map of (a) Temperature (^{o}C), (b) Nitrate concentration (μM l^{-1}), (c) [Chl a] (mg m^{-3}), and (d) $a_{\varphi}(443)/a_{\varphi}(675)$ for the California upwelling region (Cal9704) in April 1997.

default empirical algorithm is only used for waters with chlorophyll values greater than ~1.0 mg m^{-3}, less than 1% of the high-latitude data tested here were used during algorithm development.

Radiometric data adjustments were unnecessary for the three lowest MODIS wavelengths ($R_{rs}(412)$, $R_{rs}(443)$, and $R_{rs}(488)$) since instrument measurements were obtained within 2 nm of these wavelengths. The $R_{rs}(565)$ data, however, collected using the Bio-Optical Profiling System (n=323) during the Long Term Ecological Research (LTER) program were converted to $R_{rs}(555)$ using the equation developed in *O'Reilly et al.,* [1998].

Data collected at low solar elevations with zenith angles greater than 70° were omitted. Also omitted were stations flagged with low R_{rs} values ($R_{rs}(412) < 0.0008$ sr^{-1} and $R_{rs}(551) < 0.001$ sr^{-1}) or with inconsistent empirical and semi-analytic chlorophyll values. When the fully packaged parameter set was applied, the semi-analytical and empirical output products ([chl a], $a_{\varphi}(675)$, $a_{g}(400)$) were blended according to Equation 14 when the semi-analytic algorithm returned $a_{\varphi}(675)$ values between 0.0075 and 0.015 m^{-1}. This differs from the range used for unpackaged date (0.015 - 0.030 m^{-1}) as a result of the lower chlorophyll-specific absorption coefficient observed in high-latitude waters compared to mid- and
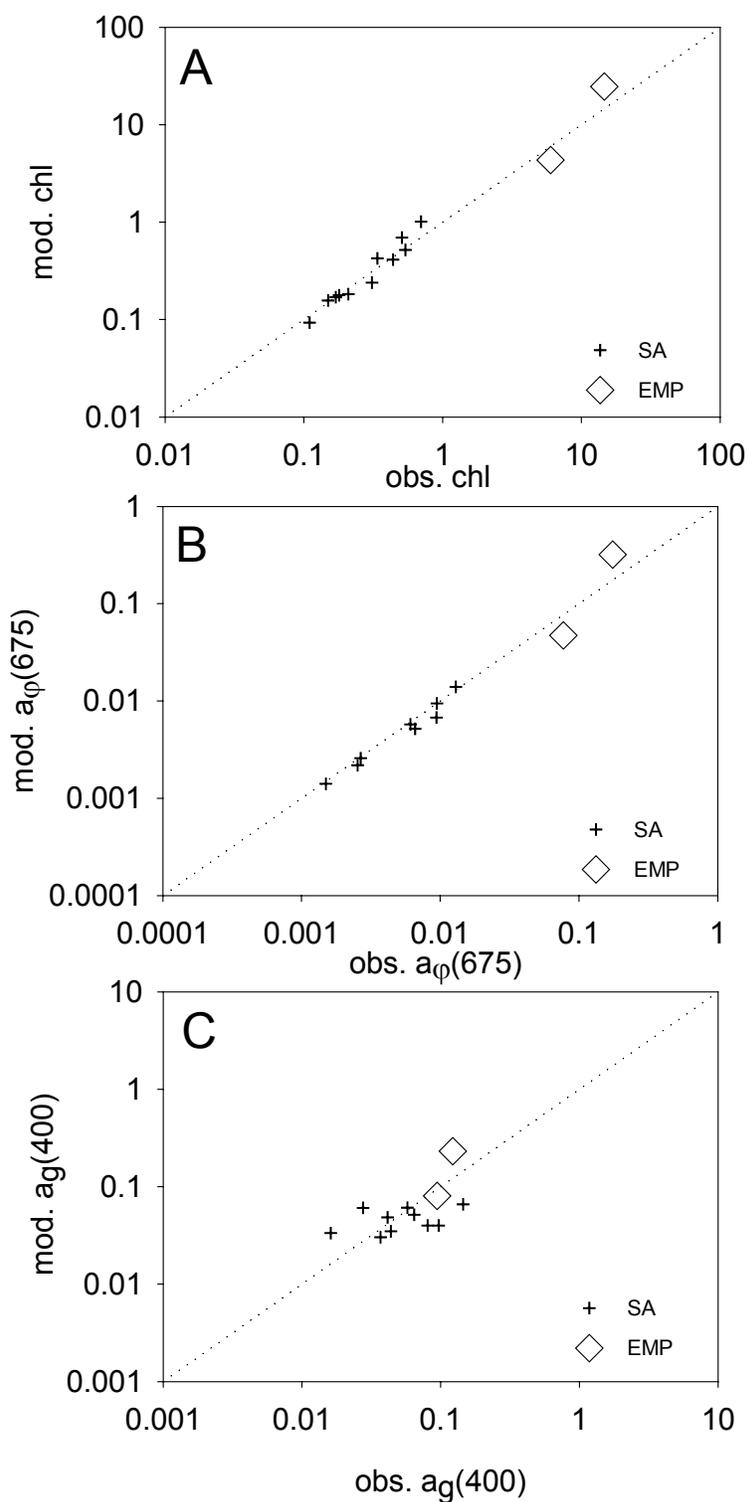
Figure 16. Algorithm performance for domain-sorted California upwelling data (Cal9704) (a) observed versus modeled [chl *a*], (b) observed versus modeled $a_\varphi(675)$, and (c) observed versus modeled $a_g(400)$. The lines are one-to-one lines, SA (+) indicates points that are calculated semi-analytically or by a blend of semi-analytical and empirical values, while EMP (◊) indicates points that are calculated empirically.

low-latitude waters.

The Antarctic data (ROAVERRS97, NBP9711, REV9801, REV9802, AMLR2000, AMLR2001, and LTER) consist of R_{rs} values determined from subsurface upwelling radiance extrapolated to just below the surface, $L_u(0^-,\lambda)$, and downwelling irradiance extrapolated to just below the sea surface, $E_d(0^-,\lambda)$. Remote-sensing reflectance just above the sea surface, $R_{rs}(0^+,\lambda)$, was calculated using the following equation:

$$R_{rs}(0^+,\lambda) \approx \frac{0.54\, L_u(0^-,\lambda)}{1.04\, E_d(0^-,\lambda)} \qquad (20)$$

where 0.54 and 1.04 are transfer coefficients across the air-sea interface for L_u and E_d, respectively [*Austin,* 1974]. All of the Antarctic data except for that collected during the AMLR2000 and AMLR2001 cruises are corrected for ship shadow effects.

The spring Bering Sea data set (MF0796) includes hyperspectral $R_{rs}(\lambda)$ measurements collected just above the sea surface and processed according to *Lee et al.,* [1996]. Cota's Bering Sea (Ber96), Labrador Sea (Lab96, Lab97, and Lab00), and the Gulf of Alaska (Goa97) R_{rs} data were calculated using Equation 20 from subsurface $L_u(\lambda)$ and $E_d(\lambda)$ data.

The *in situ* chlorophyll concentrations for the entire high-latitude data set ranged between 0.06 and 40 mg m^{-3}. Mean and median values for the Antarctic data are 2.9 mg m^{-3} and 1.4 mg m^{-3}, respectively. Similar values for the Arctic data (2.5 mg m^{-3} and 1.5 mg m^{-3}, respectively) were observed. Data collected in the Southern Ocean represent the majority (92%) of the high-latitude data set. Most of these data (87%) were collected west of the Antarctic peninsula (LTER) between 1991 and 1999 and over 95% of the data were collected between November and February. Since the majority of the Antarctic data were collected either near coastal polynas greatly influenced by sea ice meltwater (i.e. Ross Sea) or adjacent to continental margins (i.e. north and west of the Antarctic peninsula), the Antarctic data set over emphasizes bloom-dominated regions and under emphasizes oligotrophic regions influenced by the major circumpolar currents.

6.3.2 Antarctic data

Compared to the two-band empirical CZCS algorithm [*Gordon et al.,* 1983], the Antarctic data exhibited higher $R_{rs}(443)/R_{rs}(551)$ ratios on average for a given chlorophyll concentration (Figure 17d). This may be attributed to lower $a_\varphi^*(\lambda)$ due to increased pigment packaging, decreased chlorophyll-specific detrital and CDOM absorption, and decreased chlorophyll-specific backscattering compared to northern mid- and low-latitude data where the CZCS algorithm was developed [*Sosik et al.,* 1992; *Dierssen and*
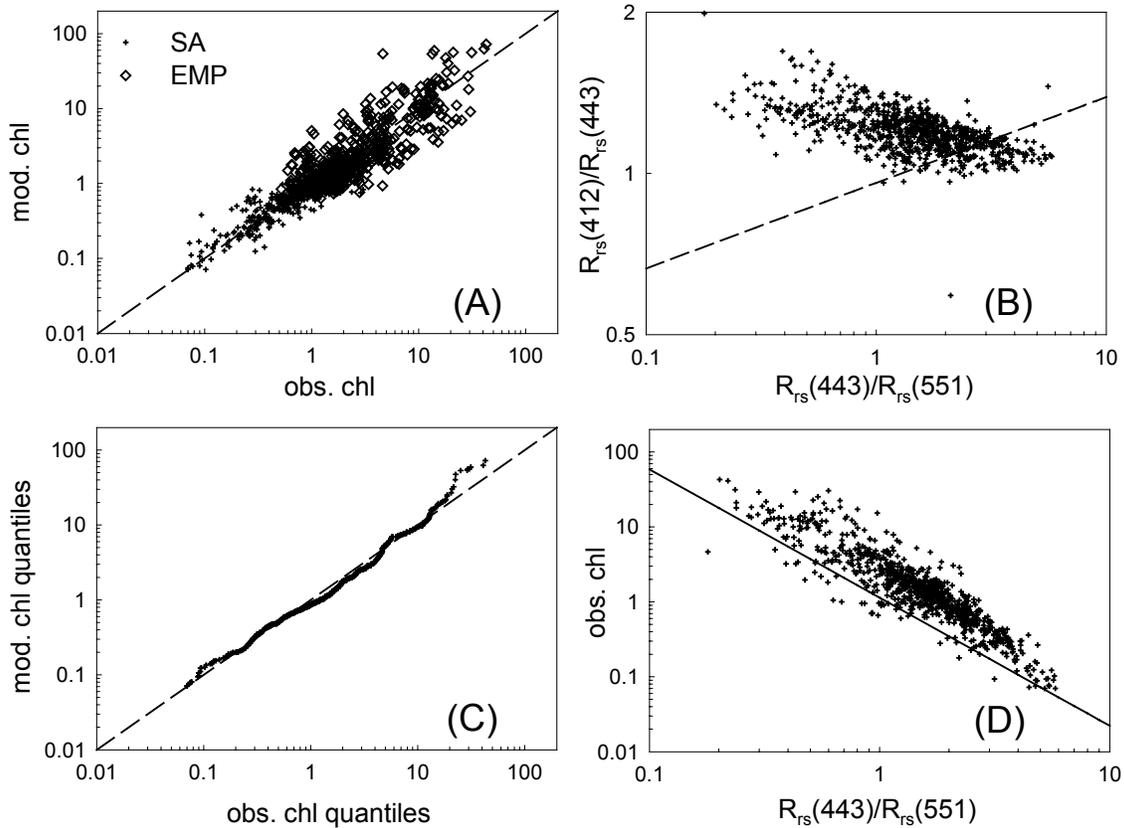
Figure 17. Algorithm performance for and analysis of the Antarctic data set. (a) Scatterplot of observed versus modeled chl *a* (mg m^{-3}) calculated semi-analytically ($+$) and empirically ($\Diamond$). The dashed line is the one-to-one line. (b) The r_{12} versus r_{25} relationship with the line, $r_{12} = 0.95[r_{25}]^{0.16}$. (c) Quantile-quantile plot of observed versus modeled chl *a*. (d) Observed chl *a* versus r_{25}, with the Coastal Zone Color Scanner (CZCS) algorithm line $C=1.14\ [r_{25}]^{-1.71}$.

Smith, 2000; *Reynolds et al.,* 2001]. The first two factors would result in elevated $R_{rs}(443)$ values while the third factor would result in decreased $R_{rs}(551)$ values.

Lower chlorophyll-specific detrital and CDOM absorption relative to values from northern mid- and low-latitude waters is also evident in the high $R_{rs}(412)/R_{rs}(443)$ ratios exhibited at high chlorophyll concentrations (or low $R_{rs}(443)/R_{rs}(551)$ ratios) using the second numerical filter discussed in Section 4.3.2 (Figure 17b). The $R_{rs}(412)/R_{rs}(443)$ ratios are higher than those observed in the global data set (Figure 9b) as CDOM and detrital absorption increase at a slower rate with increasing chlorophyll concentration causing $R_{rs}(443)$ to decrease faster than $R_{rs}(412)$. At low chlorophyll concentrations (or high $R_{rs}(443)/R_{rs}(551)$ ratios), the Antarctic data fall mostly below the line $r_{12}=0.95[r_{25}]^{0.16}$ similar to the Southern California upwelling data (Figure 8b) and are consistent with pigments derived from a highly packaged pigment domain.

Since sea-surface temperatures were not available for the Antarctic data set, the semi-analytic algorithm was run using the fully packaged parameter set only. The scatterplot of measured versus

modeled chlorophyll concentrations overlies the one-to-one line (Figure 17a). Similarly, the quantile-quantile plot (Figure 17c), though sinuous, overlies the one-to-one line quite well for chlorophyll concentrations less than 10 mg m^{-3}. At chlorophyll concentrations greater than 10 mg m^{-3}, the increased scatter and bias may be attributed to the unique optical signatures associated with monospecific blooms (i.e. Figure 13) and is most likely the main reason why the default empirical algorithm fails to perform accurately here.

Processing the Antarctic data using the SeaWiFS OC4 (version 4) empirical algorithm [*O'Reilly et al.,* 2000] results in significant underestimations of chlorophyll concentration between ~0.2 and 10 mg m^{-3}. Errors such as this are readily apparent using graphical algorithm evaluation criteria (Figure 18). Statistically, however, the RMS2 error generated from non-log-transformed data is erroneously low due to the large bias (-0.267) that exists between the modeled and measured data (Table 7). Since the RMS2 error (Equation 17) does not place equal weight on underestimates as on overestimates, and fails to provide the same error estimate when regressing X against Y as when regressing Y against X, we now linearize the RMS1 error generated from log-transformed data as follows

$$RMS_{lin} = 0.5 \cdot [(10^{RMS}-1)+(1-10^{-RMS})] \tag{21}$$

The RMS1, RMS2, and RMS$_{lin}$ chlorophyll retrieval errors for the Antarctic data (n=871) using the semi-analytic algorithm were 0.22, 0.72, and 0.53, respectively. The RMS1, RMS2, and RMS$_{lin}$ errors using the SeaWiFS OC4v4 algorithm for the Antarctic data were 0.35, 0.60, and 0.89, respectively. Note, once again, that the RMS2 error is erroneously low when using the OC4v4 algorithm compared to when applying the semi-analytic algorithm due to the aforementioned large bias. This bias causes the linearized fractional error, RMS$_{lin}$, for OC4v4 to be ~170% higher than that for the semi-analytical algorithm. A bias of 27% for OC4v4 indicates that SeaWiFS-derived chlorophyll concentrations may perhaps be 25-30% low during austral summer which could result in similar underestimations of primary production and CO_2 uptake for the Southern Ocean.

6.3.3 Arctic data

The Arctic data are similar to the Antarctic data when plotting chlorophyll *a* concentration versus $R_{rs}(443)/R_{rs}(551)$ (Figure 19d). The majority of the stations had higher reflectance ratios for a given chlorophyll concentration compared to the CZCS algorithm [*Gordon et al.*, 1983]. Coastal stations in the Labrador Sea that were dominated by diatoms exhibited reflectance ratios that deviated the most from the CZCS line. Compared to the open-ocean stations in this region, the waters were colder and less saline
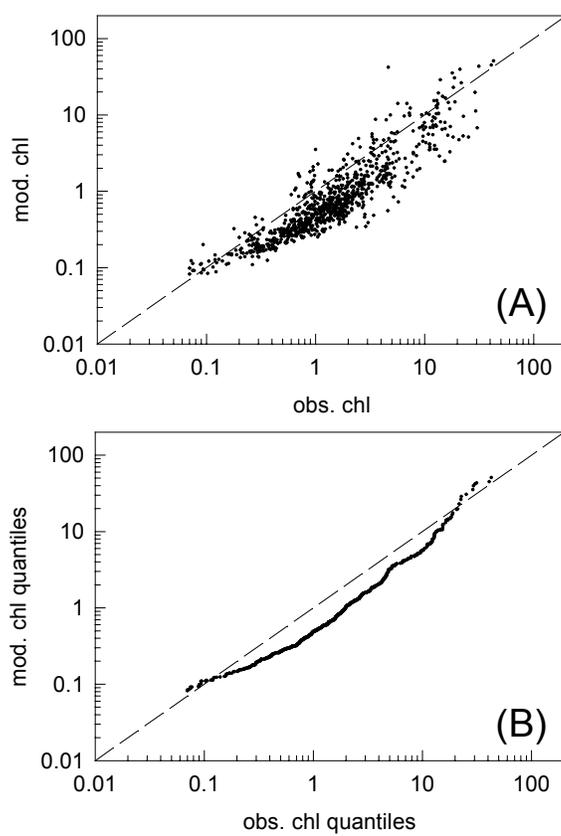
Figure 18. SeaWiFS OC4v4 algorithm performance for the Antarctic data set. (a) Scatterplot of observed versus modeled chl *a* (mg m^{-3}). The dashed line is the one-to-one line. (b) Quantile-quantile plot of observed versus modeled chl *a*.

perhaps due to ice-edge melting. Also, chlorophyll-specific phytoplankton absorption coefficients were relatively low and consistent with other studies of diatom-dominated waters in this region [*Lutz et al.,* 1996].

The spring Bering Sea data (MF0796) also exhibited relatively high reflectance ratios for data collected offshore of the 100m isobath with $a_g(443)/a_{ph}(443)$ ratios less than 2. Spring stratification due to increased thermal heating and decreased wind mixing events had not yet occurred. Vertical profiles of temperature and salinity exhibited a well-mixed water column indicative of nutrient-replete conditions and favoring the growth of large, shade-adapted diatoms containing heavily packaged pigments (Figure 12) [*Goering and Iverson,* 1981]. Stations located inshore of the 100m isobath with $a_g(443)/a_{ph}(443)$ ratios greater than 2, however, exhibited reflectance ratios more consistent with the CZCS line. Such a tendency for increased pigment packaging to increase blue-to-green reflectance ratios but then be offset by increased $a_g(443)/a_{ph}(443)$ ratios that decrease reflectance ratios is also evident in model simulations [*Sathyendranath et al.,* 2001].

The summer Bering Sea (Ber96) and the fall Gulf of Alaska (Goa97) $R_{rs}(443)/R_{rs}(551)$ ratios overlie the CZCS line (Figure 19d). These data were collected in highly stratified waters with surface mixed layers ~20m deep. Surface nutrient concentrations were depleted and daily solar fluxes were sufficient to favor the growth of picoplankton over microplankton [*Odate,* 1996]. These nutrient-efficient and high-light-adapted phytoplankton species with higher chlorophyll-specific absorption coefficients due to decreased pigment packaging and increased photoprotective carotenoids are somewhat more similar to phytoplankton assemblages observed in coastal waters used in part to generate the CZCS algorithm.
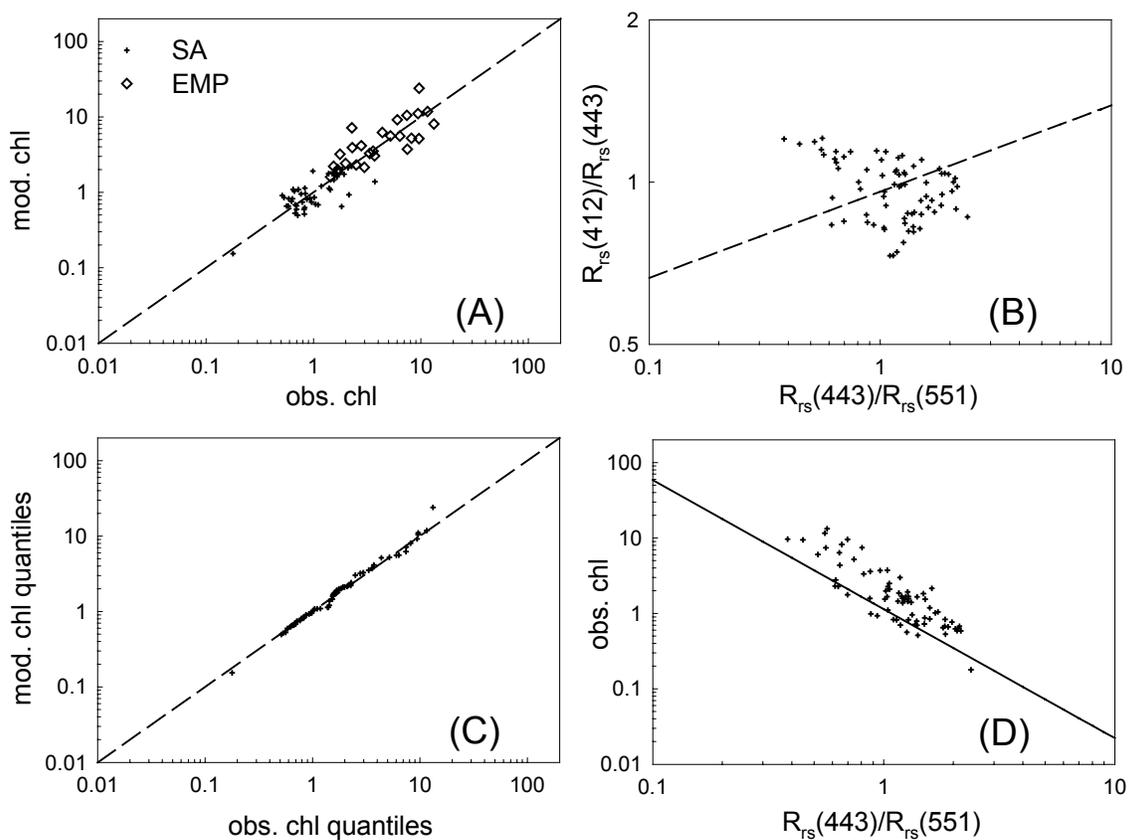
Figure 19. Algorithm performance for and analysis of the Arctic data set. (a) Scatterplot of observed versus modeled chl a (mg m^{-3}) calculated semi-analytically (+) and empirically (◊). The dashed line is the one-to-one line. (b) The r_{12} versus r_{25} relationship with the line, $r_{12} = 0.95[r_{25}]^{0.16}$. (c) Quantile-quantile plot of observed versus modeled chl *a*. (d) Observed chl *a* versus r_{25}, with the Coastal Zone Color Scanner (CZCS) algorithm line C=1.14 $[r_{25}]^{-1.71}$.

Chlorophyll-specific CDOM absorption was relatively low for Labrador Sea data and spring Bering Sea data collected offshore of the 100m isobath. The chlorophyll versus $a_g(400)$ relationship for these waters was lower than the relationship discussed in Section 4.3.2 for separating gelbstoff-rich mid- and low-latitude waters, but higher than that observed for Southern Ocean waters [*Reynolds et al.,* 2001]. As a result, $R_{rs}(412)/R_{rs}(443)$ ratios for these waters (Figure 19b) were higher than the nearshore

(gelbstoff-rich), spring Bering Sea data, but lower than the Antarctic data (Figures 17b).

As the Arctic data set encompasses a wide range of bio-optical domains ranging from the deeply-mixed (light-limited and nutrient replete), spring Labrador Sea to the highly stratified (high-light and nutrient depleted), summer Bering Sea, the data were sorted based on nitrate-depletion temperatures to determine the appropriate level of pigment packaging prior to applying the semi-analytic algorithm. Although the correlation between nitrate concentration and temperature may be weak in high-latitude oceanic waters [*Cota et al.*, 2000] since other factors (i.e. light, Si, Fe, etc.) may be responsible for limiting phytoplankton biomass accumulation, we believe that deviations is sea surface temperatures from nitrate depletion temperatures are also indicative of the degree of water-column stratification. Increased water column stratification may decrease the level of pigment packaging by maintaining the phytoplankton in a higher light environment near the surface. For instance, if phytoplankton found in high-latitude waters are light-limited rather than nutrient-limited, then the increased vertical stratification that occurs during late spring due to increased solar insolation, decreased wind stress, and in some cases increased ice-edge melting would reduce this light-limitation [*Sverdrup,* 1953; *Maynard and Clark,* 1987; *Mitchell et al.,* 1991]. The ratio of photo-protective carotenoids to chlorophyll *a* would increase resulting in higher chlorophyll-specific phytoplankton absorption coefficients [*Bricaud et al.,* 1995] typical of a less packaged pigment domain (i.e. summer Bering Sea).

The scatterplot of measured versus modeled chlorophyll concentration (Figure 19a) overlies the one-to-one line, and the quantile plot (Figure 19c) is linear and overlies the one-to-one line. The three semi-analytically derived outliers (Figure 19a) are from coastal Labrador Sea stations (Lab97). Chlorophyll-specific absorption coefficients for these stations were very low. Sea-surface temperature and salinities were also low, perhaps indicative of more optically complex ice-edge meltwaters. Although the algorithm fails to perform well here, algorithm performance in the more areal-rich open-ocean waters was good.

The RMS1 and RMS$_{lin}$ errors for the Arctic data (n=75) using the semi-analytical algorithm were 0.17 and 0.41, respectively (Table 7). Processing the data using the SeaWiFS OC4v4 algorithm resulted in larger RMS1 and RMS$_{lin}$ errors of 0.22 and 0.54, respectively. These larger errors are primarily due to the large bias (-0.143) exhibited when using this empirical algorithm. The higher blue-to-green reflectance ratios for these data lead to significant underestimations of chlorophyll concentrations similar to those found for the Antarctic data.

7.0 Satellite data

SeaWiFS radiance imagery has been used with the *Carder et al.*, [1999] semi-analytic (SA) code for an upwelling site [*Smyth et al.,* 2001] and for a river-plume site [*Hu et al.,* 2003]. In the upwelling

case OC4 retrievals underestimated the high-chlorophyll values while the SA retrievals were much more accurate. For the river-plume case OC4 retrievals overestimated chlorophyll for gelbstoff-rich regions by as much as a factor of 2. The SA code with global parameters was generally within 35% of field values except where the absorption was dominated by gelbstoff, where mean error increased to about 41%.
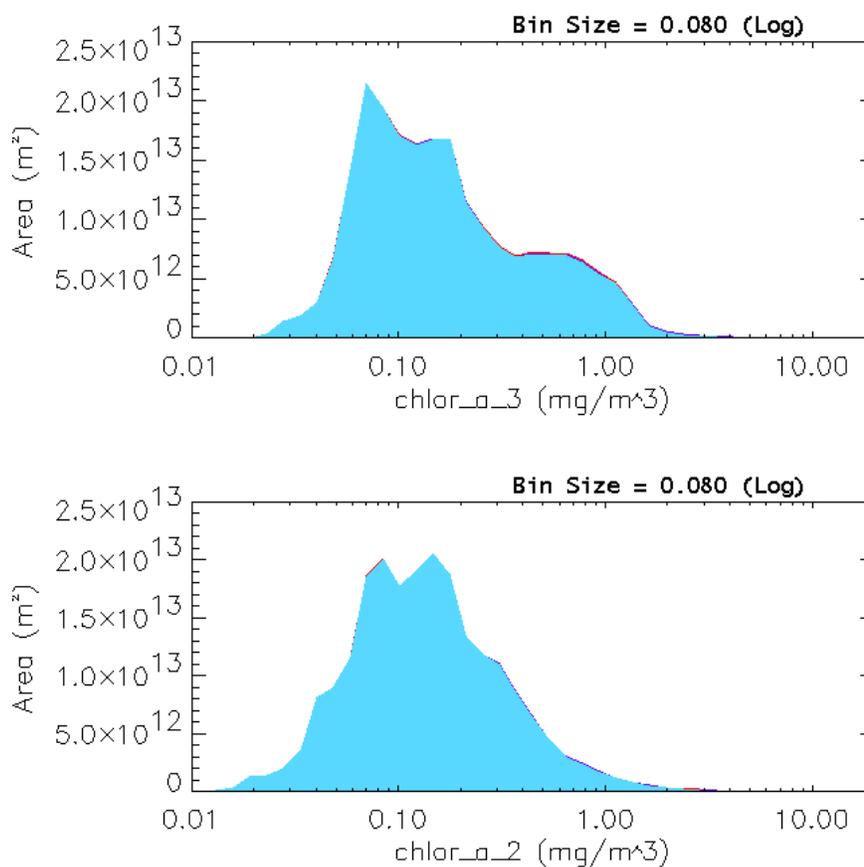
Figure 20. Histograms of weekly mean global chlorophyll concentration from MODIS for the week beginning 8 November 2000: (top) Chlor_a_3 and (bottom) Chlor_a_2 retrievals (courtesy MODIS Quality Assurance Browse Imagery, Terra collection 4). Mean values are 0.325 mg m^{-3} for Chlor_a_3 and 0.214 mg m^{-3} for Chlor_a_2. Note the differences above 0.30 mg m^{-3}.

Using the MODIS Team-Leader computing facility (MODAPS), retrieved data with Version 4.0 of the MODIS ocean processing code are compared for Chlor_a_3 and Chlor_a_2 algorithms. Chlor_a_2 is designed to be a MODIS surrogate for OC4 (see Dr. Janet Campbell's ATBD update). It can't be exactly the same as OC4 because the 510 nm SeaWiFS band is unavailable using MODIS data. Comparing retrievals from the two algorithms for MODIS Terra global data, composite-averaged over the week starting 8 November 2000 (Figure 20), three modal values are apparent in Chlor_a_3 data at the following values: 0.07, 0.18, and 0.60 to 1.2 mg m^{-3}. Chlor_a_2 modal values are found at 0.08 and 0.15

mg m^{-3}, suggesting similar mean values in the oligotrophic central gyres, but reduced Chlor_a_2 values for more eutrophic waters. With no third mode for Chlor_a_2, its global mean value (0.214 mg m^{-3}) is roughly 2/3 the global mean value (0.325 mg m^{-3}) provided by Chlor_a_3. This underestimate is consistent with low SeaWiFS OC2 retrievals [*Moore et al.,* 1999] and a 27% negative bias for OC4 retrievals (see Figure 18) for the Southern Ocean field data. This example represents a period of time (e.g. fall bloom for the northern hemisphere and spring bloom for the Southern Ocean) when the weakness of the SeaWiFS OC2 and OC4 algorithms is most apparent. Note that historical, fall, globally averaged chlorophyll *a* values are 0.305 mg m^{-3} [*Gregg and Conkright,* 2001], very close to the Chlor_a_3 value.
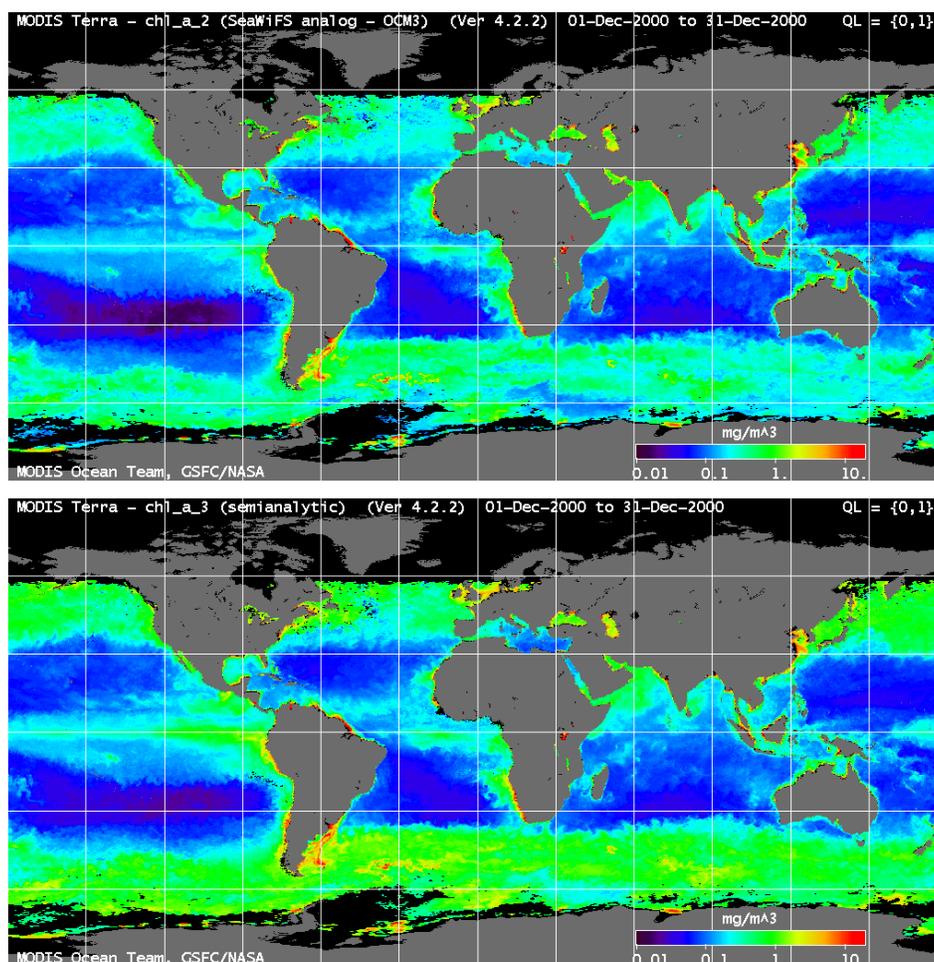
Figure 21. Global compisited maps (December 2000) of chlorophyll a concentration (mg m^{-3}) retrieved using empirical (Chlor_a_2; top) and semi-analytic (Chlor_a_3; bottom) algorithms from MODIS Terra radiometry.

MODIS Terra chlorophyll images from the GESDAAC (Goddard Earth Science Distributed Active Archive Center) for Chlor_a_2 and Chlor_a_3 were composited in 39 km bins for December 2000 and are shown in Figure 21. The subtropical gyre regions appear similar for the two images, and the

northern modal retrievals (0.087 mg m^{-3}) and southern modal retrievals (0.078 mg m^{-3}) for the two algorithms are essentially the same. However, the global mean value for Chlor_a_3 (0.294 mg m^{-3}) is higher than for Chlor_a_2 (0.231 mg m^{-3}) because in part the high-latitude and equatorial upwelling regions for Chlor_a_3 are richer in chlorophyll *a*.

Figure 22 shows that monthly mean values for Terra Chlor_a_2 and Chlor_a_3 are similar from March to June for austral fall for the southern hemisphere, but Chlor_a_2 is only 60% of Chlor_a_3 during austral spring, largely due to the package effect. Chlor_a_3 values are larger for northern spring data, but smaller during summer and fall. Gelbstoff-rich runoff from northern rivers enrich summer water color, apparently increasing perceived chlorophyll retrieved by Chlor_a_2. Chlor_a_3 spectrally partitions this type of component from chlorophyll *a*, effectively minimizing the influence of river runoff on pigment overestimates.
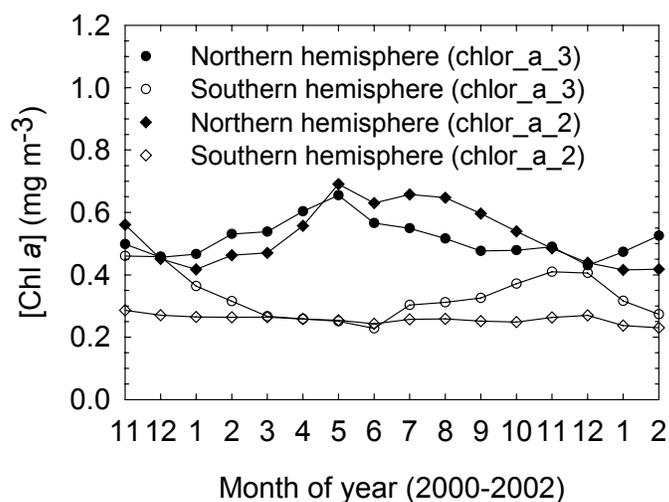
Figure 22. MODIS (reprocessed, Collection-4) Chlor_a_3 and Chlor_a_2 monthly means for Northern and Southern hemispheres from Nov-2000 and Feb-2002.

The validity of Chlor_a_2 and Chlor_a_3 data was evaluated using match-ups with ship data from the SeaWiFS SeaBASS data archive [*Werdell and Bailey*, 2002]. Chlorophyll imagery from MODIS Terra was compared to ship data following the general match-up exclusion protocol of *McClain et al.*, [2000], but only quality-level zero MODIS chlorophyll *a* data were used. This eliminated data from shoal areas (< 30 m) and provided cloud-free data collected within three hours of the satellite overpass. Furthermore, for selected pixels within 100 pixels of the scene edge, 5-by-5 pixel means rather than traditional 3-by-3 median values were used to improve signal-to-noise ratios. Field chlorophyll values within the top 10 meters were averaged for comparison with satellite retrievals.

Global match-up results are presented in Figure 23 for the Antarctic, Equatorial Pacific,

California Current, western mid-Pacific, and the West Florida Shelf. Note that both Chlor_a_2 (RMS = 0.174) and Chlor_a_3 (RMS = 0.170) are accurate to less than 1/5 log unit, more accurate than the OC4v4 algorithm (RMS=0.222) update [*O'Reilly et al.,* 2000] using an expanded global field of data. Ideally, for a 1:1 line, A=B=1.0. Although the RMS error values for the two algorithms are similar, Chlor_a_3 values for A and B are much closer to 1.0. This suggests that the error due to overestimates by Chor_a_2 at low values and underestimates at high values are comparable to additional scatter about the line associated with Chlor_a_3.
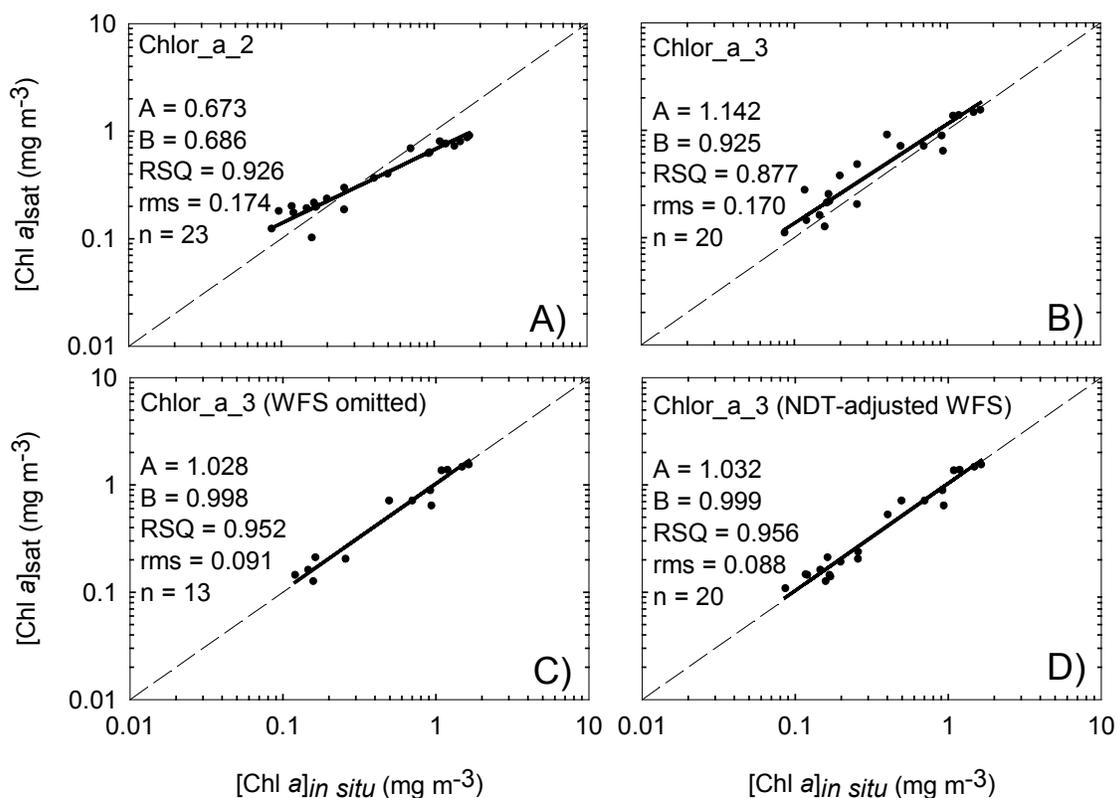
Figure 23. Relationships between *in situ* [Chl *a*] and MODIS-derived [Chl *a*] using a) Chlor_a_2, b) Chlor_a_3, c) Chlor_a_3 without the West Florida Shelf (WFS) points, and d) Chlor_a_3 with the WFS points that have been NDT-adjusted. Dashed lines are one-to-one lines and solid lines are linear regression lines in log-log coordinates.

The error is reduced to 0.091 for Chlor_a_3 by removing the seven West Florida Shelf (WFS) points. In fact continental shelves with terrigenous runoff are not expected to exhibit typical NDT behavior. For the West Florida Shelf, upwelling of $18\text{-}20^0$ C from below the Loop Current region is not unusual [*Austin,* 1970; *Haddad and Carder,* 1979], and convective overturn of surface waters in the winter is expected to refresh nutrients with water having similar thermal properties. We found that using an NDT=19.5^0 C for the seven WFS data points in the match-up data set provided the best algorithm

accuracy, lowering the error estimate when WFS points are included to RMS=0.088, or less than 1/10 of a log unit. This suggests, then, that data sets rich in continental shelf data points should be scrutinized on a regional basis. If that is not possible, shelf data can be addressed using a default "global" parameter set such as given in *Carder et al.,* [1999], that minimizes extreme excursions due to the package effect.

The RMS$_{lin}$ values for data in Figure 23 calculated using Equation 21 are 41%, 40%, 21%, and 20%, respectively. These results are excellent, with nearly all values reaching the 35% goal set for MODIS chlorophyll *a* accuracies. Without stations from continental shelves, the accuracies easily surpass goal values for Chlor_a_3. With local NDT adjustments for coastal stations, sub-25% error values also appear attainable from Chlor_a_3.

Although validation stations encompass a wide range of environmental settings, with chlorophyll concentrations ranging from ~0.1 to 1.5 mg m^{-3}, data from many parts of the ocean and especially the central gyre regions are yet to be assessed. Initial results from January to June 2001, however, are very encouraging, especially for upwelling (California Current and equatorial Pacific) and high-latitude (Antarctic) locations. The data quality for normalized water-leaving radiance values [*Gordon,* 2002] from November 2000 to February 2002 are valid at Stage 1. For this reason the validity of chlorophyll retrievals presented here is likely to also extend from November 2000 to February 2002 except perhaps for river-fed continental shelf regions.

A final observation is that detector striping, mirror side-banding, and polarization effects all can contribute to errors in MODIS data, although the effects were reduced by at least a factor of five in Collection 4. These are more likely to be apparent at the edge of high-resolution scenes abutting adjacent scenes, where different view angles compound the differences observed in residual effects due to atmospheric and polarization corrections. The 5-km binning of match-up imagery for comparison to field data at scene edges reduces the detector- striping and side-banding effects, and residual effects are not apparent in weekly or monthly 39 km composites of data used in global primary production estimates [*Esaias et al.,* 2002].

8.0 Conclusions

A MODIS semi-analytical algorithm for chlorophyll *a* was tested using a total of 976 global data points from regions where the pigments were typically unpackaged, packaged, or transitional with appropriate algorithm parameters applied for each data type. This resulted in "Version 1" of the semi-analytic algorithm [*Carder et al.,* 1999], which did not address the high-latitude regions with extremely packaged pigments (termed "fully packaged") which are included in "Version 2" of the semi-analytic algorithm. The algorithm has thus evolved to better represent the entire global data set.

The "unpackaged" type consisted of data sets that were generally consistent with the case 1 CZCS

algorithm and contained mostly tropical, subtropical, and summer temperate data. This algorithm type was parameterized using Gulf of Mexico and Arabian Sea data, and it continues to remain the same in both Version 1 and Version 2 of the algorithm. The Version 1 "packaged" type of pigment-absorption parameterization was consistent with pigments found in eastern-boundary upwelling data sets containing somewhat more packaged pigments, but not consistent with the fully packaged pigments found in high-latitude data. Note that at times for upwelling centers, some of the phytoplankton have pigments that are as highly packaged as found in high-latitude data sets, but that is not true for the general region. The packaged data sets studied with Version 1 were processed with the algorithm modified for phytoplankton-absorption parameters consistent with the Southern California Bight area. This resulted in two fairly equally divided data sets totaling 604 points. That left 372 data points that were not well enough characterized to classify.

The Version 1, semi-analytical (SA) algorithm for chlorophyll a performed well on each of the data sets after classification, resulting in RMS1 errors of 0.099 and 0.111 (e.g., 0.10 log unit) for the unpackaged and packaged data classes, respectively, with little bias and with slopes near 1.0. RMS2 linearized errors for the algorithms were 23% and 27% for the two classes, respectively. The SA algorithm for phytoplankton absorption provided data accurate to about 30%.

While these numbers are excellent, one must bear in mind what misclassification does to the chlorophyll results. Using parameters for an average or transitional domain in the semi-analytical MODIS algorithm with the global data set (n=976) yielded an RMS2 error of 44.6%, while applying the unpackaged parameters on the global evaluation data set yielded an RMS2 error of 92%. So, without classification, the algorithm performs better globally using the average parameters than it does if misclassification occurs.

For the difficult transition period between spring and summer or the regions between upwelling centers and the warmer offshore waters, a data set was tested that included the eastern boundary region of the North Atlantic. Nitrogen-depletion temperatures were used with AVHRR-derived sea-surface temperatures to sort stations into packaged, unpackaged, and transitional domains. Comparing sea-surface temperature (SST) to the nitrate-depletion temperature (NDT) provides a means of estimating how packaged were the pigments for a given pixel. Cold SST values relative to NDTs suggest convective overturning or upwelling has brought cold, nutrient-rich water to the surface. Phytoplankton in these waters are typically large, contain high ratios of chlorophyll pigment per cell because they have recently experienced very low light levels, and exhibit low chlorophyll specific absorption coefficients. Solar heating warms this water, reduces the cell requirement for light-harvesting pigments including chlorophyll a while increasing the cell requirement for photo-protective pigments, decreases the size of cells that can remain neutrally buoyant, and results in an increase in the chlorophyll specific absorption

coefficient.

RMS2 errors dropped from 50% to 38% as a result of this data-sorting exercise. Since large regions of the subtropical and tropical Atlantic, Pacific, and Indian Oceans remain in the unpackaged bio-optical domain during all seasons and provide stable data accuracies from 24% to 28%, it is reasonable to expect that use of an NDT-based sorting algorithm with MODIS sea-surface temperatures to separate data into appropriate bio-optical domains will result in accuracies for the MODIS semi-analytical chlorophyll *a* algorithm that are significantly lower than our target value of 35%.

This completed the evaluation of mid- to low- latitude data sets considered for Version 1 of the algorithm and used in Collections 1 through 3 for ocean data found in the MODIS Data Active Archive Computer (DAAC) at NASA Goddard. Version 2 of the algorithm is discussed below and is used in Collection 4 of the ocean data found in the DAAC. Version 2 is summarized below.

In Version 2, "fully packaged" pigment parameters were derived from high latitude polar and temperate upwelling data sets to replace the previously designated "packaged" parameter set. In addition, a smoother strategy for transitioning from the unpackaged to the fully packaged pigment domain was introduced using sea surface temperatures and nitrate depletion temperatures. These transitions can be thought of as transitions between fall and winter (fall overturn) and spring and summer (spring bloom) or as transitions between upwelling and offshore waters.

The 5° C range between unpackaged-pigment conditions (warm waters) and conditions of fully packaged pigments, provides a means of transitioning algorithm parameterization between the two extremes using the weighted average of chlorophyll retrievals from the two based upon SST-NDT values from -1° C to 4° C. Tests in the Southern California Bight transition region between upwelled and offshore waters indicate that errors are reduced from 39 to 31% using this method for transitioning between packaging domains.

Compared to the SeaWiFS OC4 empirical algorithm, application of the MODIS Chlor_a_3 semi-analytical algorithm to Southern Ocean field data reduced the error in deriving chlorophyll concentration by almost a factor of two. Accuracy tests using MODIS satellite data for November 2000 show that Chlor_a_3 retrievals of global mean chlorophyll *a* concentration are within 8% of the historical seasonal mean, while OC4-like empirical retrievals using Chlor_a_2 are but 2/3 of the seasonal mean. This suggests that Chlor_a_3 semi-analytical algorithm retrievals of chlorophyll *a* concentrations will lead to larger, more accurate pigment and subsequent global primary production numbers than are presently being retrieved using SeaWiFS and Coastal Zone Color Scanner data sets.

Both the Chlor_a_3 and Chlor_a_2 algorithms used with MODIS Terra (Collection 4) data provide nearly identical modal chlorophyll values for the northern (0.087 mg m^{-3}) and southern (0.078 mg m^{-3}) central gyres in December 2000. However, the global mean value for Chlor_a_3 is higher (0.294 mg

m^{-3}) than for Chlor_a_2 (0.231 mg m^{-3}). This difference can be explained by the Southern Ocean where Chlor_a_2 values are on average about half of field and Chlor_a_3 values due to lower chlorophyll-specific absorption coefficients typical of this region. MODIS Terra retrievals of chlorophyll *a* using reprocessed Collection 4 data are accurate to better than 41%. Removing data points from continental shelves improves Chlor_a_3 accuracies to 21%, while promoting shelf data using more appropriate nitrate-depletion temperatures can improve accuracies to about 20%. The higher accuracies do exceed our expectations, and only when data from more regions (e.g. southern central gyres, the southern ocean) and seasons (northern summer and fall) are included will a better idea of the actual range of accuracies be known. Then, an area-weighted global mean accuracy for each algorithm can be assessed for MODIS Terra. For MODIS Aqua performance evaluation awaits reprocessing with vicariously calibrated data.

Regional inaccuracies are expected to be higher, especially for Chlor_a_2 retrievals from upwelling and high-latitude regions, where underestimates compared to ship and Chlor_a_3 data can approach a factor of 2. Chlor_a_2 retrievals in northern waters rich in gelbstoff may somewhat overestimate Chlor_a_3 retrievals. Both algorithms are expected to be less accurate for layer systems such as river plumes and ice-melt plumes with mono-specific blooms and/or vertical structure. As more field data become available, regional accuracies with the global algorithms can be assessed, and local improvements in use of the NDT strategy can be implemented.

9.0 Output Products

Output products from MOD19 will include the following:

1. Concentration of chlorophyll *a* for concentrations from .02 to 50 mg/m^3 for optically deep waters.

2. The absorption coefficient at 400 nm , $a_g(400)$ due to gelbstoff or colored, dissolved organic matter. All absorption coefficients $a_g(\lambda)$ for $400 < \lambda < 700$ nm can then be estimated with knowledge of the spectral slope parameter S.

3. The absorption coefficient at 443 nm, $a_\varphi(443)$, due to phytoplankton; this is passed along to MOD20 for calculation of $a_\varphi(\lambda)$ for the visible spectrum as a contribution to the absorbed radiation by phytoplankton, ARP, used for fluorescence efficiency calculations.

4. The sum of $a_w(\lambda)$, $a_g(\lambda)$, and $a_\varphi(\lambda)$ provides the total absorption coefficient spectrum, $a_t(\lambda)$, and the diffuse attenuation spectrum, $k_d(\lambda) = a_t(\lambda) / \cos q_0$. See MOD20.

10.0 References

Aiken, J., G.F. Moore, C.C. Trees, S.B. Hooker, and D.K. Clark, The SeaWiFS CZCS-type pigment algorithm, in *SeaWiFS Technical Report Series*, vol. 29, edited by S.B. Hooker and E.R. Firestone, Goddard Space Flight Center, Greenbelt, MD, 1995.

Arrigo, K.R., D.H. Robinson, D.L. Worthen, B. Schieber, and M.P. Lizotte, Bio-optical properties of the southwestern Ross Sea, *J. Geophys. Res.*, 103: 21,683-21,695, 1998.

Austin, H.M., The Florida Middle Ground, *Mar. Pollution Bull.*, 2, 171-172, 1970.

Austin, R.W., Inherent spectral radiance signatures of the ocean surface, in *Ocean Color Analysis*, pp. 2.1-2.20, Scripps Institute of Oceanography, San Diego, CA, 1974.

Baker, K.S. and R.C. Smith, Bio-optical classification and model of natural waters, *Limnol. Oceanogr.*, 27, 500-509, 1982.

Barnes, R.A., W.L. Barnes, W.E. Esaias, and C.R. McClain, Prelaunch acceptance report for the SeaWiFS radiometer, in *SeaWiFS Technical Report Series*, vol. 22, edited by S.B. Hooker, E.R. Firestone, and J. G. Acker, Goddard Space Flight Center, Greenbelt, MD, 1994.

Behrenfeld, M.J. and P.G. Falkowski, Photosynthetic rates derived from satellite-based chlorophyll concentration, *Limnol. Oceanogr.*, 42, 1-20, 1997.

Bissett, W.P., J.S. Patch, K.L. Carder, and Z.P. Lee, Pigment packaging and chlorophyll *a* specific absorption in high-light oceanic waters, *Proc. SPIE Int. Soc. Opt. Eng.*, *2963*, 358-374, 1997.

Bricaud, A., A. Morel, and L. Prieur, Absorption by dissolved organic matter in the sea (yellow substance) in the UV and visible domains, *Limnol. Oceanogr.*, *26*, 43–53, 1981.

Bricaud, A., M. Babin, A. Morel, and H. Claustre, Variability in the chlorophyll-specific absorption coefficients of natural phytoplankton: Analysis and parameterization, *J. Geophys. Res. 100*: 13,321-13,332, 1995.

Brody, E., B.G. Mitchell, O. Holm-Hansen, and M. Vernet, Species-dependent variations of the absorption coefficient in the Gerlache Strait, *Antarctic Journal*, 27, 160-162, 1992.

Carder, K.L., R.G. Steward, J.H. Paul, and G.A. Vargo, Relationships between chlorophyll and ocean color constituents as they affect remote sensing reflectance, *Limnol. Oceanogr., 31*, 403-413, 1986.

Carder, K.L., R.G. Steward, G.R. Harvey, and P.B. Ortner, Marine humic and fulvic acids: Their effects on remote sensing of ocean chlorophyll, *Limnol. Oceanogr.*, *34*, 68–81, 1989.

Carder, K.L., S.K. Hawes, K.A. Baker, R.C. Smith, R.G. Steward, and B.G. Mitchell, Reflectance model for quantifying chlorophyll *a* in the presence of productivity degradation products, *J. Geophys. Res.*, *96*, 20,599–20,611, 1991.

Carder, K.L., F.R. Chen, Z.P. Lee, and S.K. Hawes, Semianalytic Moderate-Resolution Imaging Spectrometer algorithms for chlorophyll *a* and absorption with bio-optical domains based on nitrate-depletion temperatures, *J. Geophys. Res.*, 104, c3, 5403-5421, 1999.

Carder, K.L., F.R. Chen, J.P. Cannizzaro, J.W. Campbell, and B.G. Mitchell, Performance of MODIS semi-analytic ocean color algorithm for chlorophyll-*a*, *Advances in Space Research*, in press, 2003.

Clementson, L.A., J.S. Parslow, A.R. Turnbull, D.C. McKenzie, and C.E. Rathbone, Optical properties of waters in the Australian sector of the Southern Ocean, *J. Geophys. Res.*, 106, 31,611-31,625, 2001.

Cota, G.F., W.G. Harrison, T.Platt, S. Sathyendranath, and V. Stuart, Bio-optical properties of the Labrador Sea, *J. Geophys. Res.*, 2000 (submitted).

Del Castillo, C.E., P.G. Coble, R.N. Conmy, F.E. Muller-Karger, L. Vanderbloemen, and G.A. Vargo, Multispectral *in-situ* measurements of organic matter and chlorophyll fluorescence in seawater: documenting the intrusion of the Mississippi River plume in the West Florida Shelf, *Limnol. Oceanogr.*, 46, 1836-1843, 2001.

Dierssen, H.M. and R.C. Smith, Bio-optical properties and remote sensing ocean color algorithms for

Antarctic peninsula waters, *J. Geophys. Res.*, 105, 26,301-26,312, 2000.

DiTullio, G.R. and W.O. Smith Jr., Spatial patterns in phytoplankton biomass and pigment distributions in the Ross Sea, *J. Geophys. Res.*, 101, 18,467-18,477, 1996.

Esaias, W., M. Abbott, K. Carder, J. Campbell, D. Clark, R. Evans, H. Gordon, O. Brown, P. Minnett, E. Kearns, K. Kilpatrick, B.G. Mitchell, K.R. Turpie, R. Woodward, R. Vogel, D. Thomas, Ocean primary production estimates from Terra MODIS and their dependency on satellite chlorophyll *a* algorithms, Submitted to *Remote Sensing of the Environment*, 2002.

Goering, J.J. and R.L. Iverson, Phytoplankton distributions on the southeastern Bering Sea shelf, In *The Eastern Bering Sea Shelf: Oceanography and Resources*, D.W. Hood and J.A. Calder, ed., OMPA/NOAA. Distributed by University of Washington Press, Seattle, Vol.2, 933-946,1979.

Goffart, A., G. Catalano, and J.H. Hecq, Factors controlling the distribution of diatoms and *Phaeocystis* in the Ross Sea, *J. Marine Systems*, 27, 161-175, 2000.

Gordon, H.R., 2002, MODIS Science Team Algorithm Theoretical Basis Document: Normalized Water-Leaving Radiance, http://modis-ocean.gsfc.nasa.gov/qual.html/dataqualsum.V4.html.

Gordon, H.R., and A. Morel, *Remote Assessment of Ocean Color for Interpretation of Satellite Visible Imagery: A Review*, Springer-Verlag, New York, 1983.

Gordon, H.R., and M. Wang, Retrieval of water-leaving radiance and aerosol optical thickness over the ocean with SeaWiFS: A preliminary algorithm, *Appl. Opt., 33,* 443-452, 1994.

Gordon, H.R., O.B. Brown, and M.M. Jacobs, Computed relationships between the inherent and apparent optical properties of a flat homogeneous ocean, *Appl. Opt.*, *14*, 417–427, 1975.

Gordon, H.R., D.K. Clark, J.W. Brown, O.B. Brown, R.H. Evans, and W.W. Broenkow, Phytoplankton pigment concentrations in the Middle Atlantic Bight: Comparison of ship determinations and CZCS estimates, *Appl. Opt.*, *22*, 20–36, 1983.

Gordon, H.R., O.B. Brown, R.H. Evans, J.W. Brown, R.C. Smith, K.S. Baker, and D.K. Clark, A semi-analytic model of ocean color, *J. Geophys. Res.*, *93*, 10,909–10,924, 1988.

Gregg, W.W. and M.E. Conkright, Global seasonal climatologies of ocean chlorophyll: Blending *in situ* and satellite data for the Coastal Zone Color Scanner, *J. Geophys. Res.*, 106, 2499-2515, 2001.

Haddad, K.D. and K.L. Carder, Oceanic intrusions: one possible initiation mechanism of red tide blooms on the west coast of Florida, in *Toxic Dinoflagellate Blooms*, edited by D.L. Taylor and H.H. Seliger, pp. 269-274, Elsevier, New York, 1979.

Hawes, S.K., K.L. Carder, R.H. Evans, "MODIS CDOM and chlorophyll: a first look using SeaWiFS and AVHRR data", in *Earth Observing Systems V*, W.L. Barnes, Editor, Proc. SPIE 4135, 403-410 (2000).

Herbland, A., A. LeBouteiller, and R.Raimbault, Size structure of phytoplankton biomass in the equatorial Atlantic Ocean. *Deep Sea Res., Part A*, *32*, 819-836, 1985.

Holm-Hansen, O., and E. Riemann, Chlorophyll-*a* determinations: improvement in methodology, *Oikos*, 30, 438-447, 1978.

Hooker, S.B., C.R. McClain, J.K. Firestone, T.L. Westphal, E.-N. Yeh, and Y. Ge, The SeaWiFS bio-optical archive and storage system (SeaBASS), 1, *NASA Tech. Memo. 104566*, vol. 20, 40 pp., 1994.

Hu, C., F.E. Müller-Karger, D.C. Biggs, K.L. Carder, B. Nababan, D. Nadeau, and J. Vanderbloemen, Comparison of ship and satellite bio-optical measurements on the continental margin of the NE Gulf of Mexico, *Int. J. Rem. Sensing*, in press, 2002.

Jerome, J.H., R.P. Bukata, and J.E. Burton, Utilizing the components of vector irradiance to estimate the scalar irradiance in natural waters, *Appl. Opt.*, *27*, 4012–4018, 1988.

Kamykowski, D., A preliminary biophysical model of the relationship between temperature and plant nutrients in the upper ocean, *Deep Sea Res., Part A*, *34*, 1067–1079, 1987.

Kamykowski, D., and S.J. Zentara, Predicting plant nutrient concentrations from temperature and sigma-*t* in the upper kilometer of the world ocean, *Deep Sea Res., Part A*, *33*, 89–105, 1986.

Kirk, J.T.O., *Light and Photosynthesis in Aquatic Ecosystems*, 401 pp., Cambridge Univ. Press, New

York, 1983.

Kirk, J.T.O., Dependence of relationship between inherent and apparent optical properties of water on solar altitude, *Limnol. Oceanogr.*, *29*, 350–356, 1984.

Kirk, J.T.O., Volume scattering function, average cosines, and the underwater light field, *Limnol. Oceanogr.*, *36*, 455–467, 1991.

Lee, Z.P., K.L. Carder, S.H. Hawes, R.G. Steward, T.G. Peacock, and C.O. Davis, A model for interpretation of hyperspectral remote-sensing reflectance, *Appl. Opt.*, *33*, 5721–5732, 1994.

Lee, Z.P., K.L. Carder, R.G. Steward, T.G. Peacock, C.O. Davis, and J.L. Mueller, Remote-sensing reflectance and inherent optical properties of oceanic waters derived from above-water measurements, *Proc. SPIE Int. Soc. Opt. Eng.*, *2963*, 160–166, 1996.

Lee, Z.P., K.L. Carder, R.G. Steward, T.G. Peacock, C.O. Davis, and J.S. Patch, An empirical ocean color Algorithm for light absorption coefficients of optically deep waters, *J. Geophys. Res*., *103*, 27,967-27,978, 1998.

Lutz, V.A., S. Sathyendranath, and E.J.H. Head, Absorption coefficient of phytoplankton: regional variations in the North Atlantic, *Mar. Ecol. Prog. Ser.*, 135, 197-213, 1996.

Maynard, N.G. and D.K. Clark, Satellite color observations of Spring blooming in Bering Sea shelf waters during the ice edge retreat in 1980, *J. Geophys. Res.*, 92, 7127-7139, 1987.

McClain, C.R., R.A. Barnes, R.E. Eplee, Jr., B.A. Franz, N.C. Hsu, F.S. Patt, C.M. Pietras, W.D. Robinson, B.D. Schieber, G.M. Schmidt, M. Wang, S.W. Bailey, and P.J. Werdell, SeaWiFS Postlaunch Calibration and Validation Analyses, Part 2, *NASA Tech. Memo. 2000-206892,* Vol. 10, S.B. Hooker and E.R. Firestone, Eds., NASA Goddard Space Flight Center, 57 pp., 2000.

Mitchell, B.G., Algorithms for determining the absorption coefficients for aquatic particulates using the Quantitative Filter Technique, in *Ocean Optics X, Proc. SPIE*, *Int. Soc. Opt. Eng.*, *1302*, 137–148, 1990.

Mitchell, B.G., Predictive bio-optical relationships for polar oceans and marginal ice zones, *J. Mar. Systems*, 3, 91-105, 1992.

Mitchell, B.G., and O. Holm-Hansen, Bio-optical properties of Antarctic waters: differentiation from temperate ocean models, *Deep Sea Res.*, *Part A*, *38*, 1009–1028, 1991.

Mitchell, B.G., E.A. Brody, O. Holm-Hansen, C. McClain, J. Bishop, Light limitation of phytoplankton biomass and macronutrient utilization in the Southern Ocean, *Limnol. Oceanogr.,* 36, 1662-1677, 1991.

Mobley, C.D., Light and Water, *592 pp.,* Academic, San Diego, Calif., 1994.

Moline, M.A., B.B. Prézelin, and O. Schofield, Palmer LTER: Stable interannual successional patterns of phytoplankton communities in the coastal waters off Palmer Station, Antarctica, *Ant. J. of the United States*, 32, 151-153, 1999.

Moore, J.K., M.R. Abbott, J.G. Richman, W.O. Smith, T.J. Cowles, K.H. Coale, W.D. Gardner, and R.T. Barber, SeaWiFS satellite ocean color data from the Southern Ocean, *Geophys. Res. Lett.*, 26, 1465-1468, 1999.

Moore, L.R., R. Goericke, and S.W. Chisolm, Comparative physiology of *Synechococcus* and *Prochlorococcus*: influence of light and temperature on growth, pigments, fluorescence and absorptive properties, *Mar. Ecol. Prog. Ser.*, *116*, 259–275, 1995.

Morel, A., and Y. Ahn, Optical efficiency factors of free-living marine bacterioplankton upon the optical properties and particulate organic carbon in oceanic waters, *J. Mar. Res.*, *48*, 145-147, 1990.

Morel, A., and Y. Ahn, Optics of heterotrophic nanoflagellates and ciliates: a tentative assessment of their scattering role in oceanic waters compared to those of bacterial and algal cells, *J.Mar.Res., 49*, 177-202, 1991.

Morel, A., and A. Bricaud, Theoretical results concerning light absorption in a discrete medium and application to the specific absorption of phytoplankton, *Deep Sea Res.*, *Part A*, *28*, 1357–1393, 1981.

Morel, A., and B. Gentili, Diffuse reflectance of oceanic waters: Its dependence on Sun angle as

influenced by the molecular scattering contribution, *Appl. Opt.*, *30*, 4427–4438, 1991.

Morel, A., and B. Gentili, Diffuse reflectance of oceanic waters, II, Bi-directional aspects, *Appl. Opt.*, *32*, 6864–6879, 1993.

Morel, A., and H.R. Gordon, Report of the working group of water color, *Boundary Layer Meteorol.*, *18*, 343-355, 1980.

Morel, A., and L. Prieur, Analysis of variations in ocean color, *Limnol. Oceanogr.*, *22*, 709–722, 1977.

Morel, A., Y. Ahn, F. Partensky, D. Vaulot, and H. Claustre, *Prochlorococcus* and *Synechococcus*: A comparative study of their optical properties in relation to their size and pigmentation. *J. Mar. Res.*, *51*, 617-649, 1993.

Mueller, J.L., and R.W. Austin, Ocean optics protocols for SeaWiFS validation, revision 1, *NASA Tech. Memo. 104566*, vol. 25, 1995.

Müller-Karger, F.E., C.R. McClain, R.N. Sambrotto, and G.C. Ray, A comparison of ship and Coastal Zone Color Scanner mapped distributions of phytoplankton in the southeastern Bering Sea, *J. Geophys. Res.*, 95, 11,483-11,499, 1990.

Nelson, J.R., and C.Y. Robertson, Detrital spectral absorption: Laboratory studies of visible light effects on phytodetritus absorption, bacterial spectral signal, and comparison to field measurements, *J. Mar. Res.*, *51*, 181–207, 1993.

Odate, T., Abundance and size composition of the summer phytoplankton communities in the Western North Pacific Ocean, the Bering Sea, and the Gulf of Alaska, *J. Oceanogr.*, 52, 335-351, 1996.

O'Reilly, J.E., S. Maritorena, B.G. Mitchell, D.A. Siegel, K.L. Carder, S.A. Garver, M. Kahru, and C. McClain, Ocean color algorithms for SeaWiFS, *J. Geophys. Res.*, *103*, 24,937-24,953, 1998.

O'Reilly, J.E. S. Maritorena, D.A. Siegel, M.C. O'Brien, D. Toole, B.G. Mitchell, M. Kahru, F.P. Chavez, P. Strutton, G.F. Cota, S.B. Hooker, C.R. McClain, K.L. Carder, F. Müller-Karger, L. Harding, A. Magnuson, D. Phinney, G.F. Moore, J. Aiken, K.R. Arrigo, R. Letelier, and M. Culver, "Ocean color chlorophyll *a* algorithms for SeaWiFS, OC2 and OC4: Version 4." In: SeaWiFS Postlaunch Calibration and Validation Analyses, Part 3. *NASA Tech. Memo. 2000-206892, Vol. 11*, S.B. Hooker and E.R. Firestone, Eds., NASA Goddard Space Flight Center, Greenbelt, Maryland, 9-23.

Peacock, T.G., K.L. Carder, P.G. Coble, Z.P. Lee, and S.K. Hawes, Long-path spectrophotometer for measuring gelbstoff absorption in clear waters (abstract), *EOS, Trans., AGU*, *75*, 22, 1994.

Peacock, T.P., K.L. Carder, and R.G. Steward, Components of spectral attenuation for an offshore jet in the Coastal Transition Zone, *Eos Trans. AGU*, *69*, 1125, 1988.

Pope, R.M., and E.S. Fry, Absorption spectrum (380–700 nm) of pure water, II, Integrating cavity measurements, *Appl. Opt., 36*, 8710-8723, 1997.

Prieur, L., and S. Sathyendranath, An optical classification of coastal and oceanic waters based on the specific spectral absorption curves of phytoplankton pigments, dissolved organic matter, and other particulate materials, *Limnol. Oceanogr.*, *26*, 671-689, 1981.

Reynolds, R.A., D. Stramski, and B.G. Mitchell, A chlorophyll-dependent semianalytical reflectance model derived from field measurements of absorption and backscattering coefficients within the Southern Ocean, *J. Geophys. Res.*, 106, 7125-7138, 2001.

Roesler, C.S., M.J. Perry, and K.L. Carder, Modeling *in situ* phytoplankton absorption from total absorption spectra in productive inland marine waters, *Limnol. Oceanogr.*, *34*, 1510–1523, 1989.

Sathyendranath, S., and T. Platt, Analytic model of ocean color, *Appl. Opt., 36,* 2620-2629, 1997.

Sathyendranath, S., T. Platt, C. Caverhill, R. Warnock, and M. Lewis, Remote sensing of oceanic primary production: Computations using a spectral model, *Deep Sea Res., Part A, 36,* 431-453, 1989.

Shibata, K., Spectrophotometry of intact biological materials. Absolute and relative measurements of their transmission, reflection and absorption spectra, *J. Biochem.*, *45*, 599–623, 1958.

Siegel, D., and A. Michaels, Quantification of non-algal light attenuation in the Sargasso Sea: Implications for biogeochemistry and remote sensing, *Deep Sea Res., Part II*, *43*, 321-345, 1996.

Smith, R.C., and K.S. Baker, Optical properties of the clearest natural waters (200-800nm), *Appl. Opt.*,

20, 177-184, 1981.

Sosik, H.M., M. Vernet, and B.G. Mitchell, A comparison of particulate absorption properties between high- and mid-latitude surface waters, *Antarctic Journal*, 27, 162-164, 1992.

Sullivan, C.W., K.R. Arrigo, C.R. McClain, J.C. Comiso, and J. Firestone, Distribution of phytoplankton blooms in the Southern Ocean, *Science*, 262, 1832-1837, 1993.

Sverdrup, H.U., On conditions for the vernal blooming of phytoplankton, *J. Cons. Cons. Int. Explor. Mer*, 18, 287-295, 1953.

Werdell, P.J. and S.W. Bailey, The SeaWiFS Bio-Optical Archive and Storage System (SeaBASS): Current architecture and implementation, in *NASA/TM-2002-211617*, edited by G.S. Fargion and C.R. McClain, Goddard Space Flight Center, Greenbelt, 45 pp., 2002.

Table 1a. Wavelength-Dependent Parameters for the Semi-analytical Chlorophyll Algorithm for Regions Without Packaged Pigments.

λ	412	443	488	551
b_{bw} (m^{-1})	0.003341	0.002406	0.001563	0.000929
a_w (m^{-1})	0.00480	0.00742	0.01632	0.05910
a_0	2.20	3.59	2.27	0.42
a_1	0.75	0.80	0.59	−0.22
a_2	−0.5	−0.5	−0.5	−0.5
a_3	0.0112	0.0112	0.0112	0.0112

Table 1b. Wavelength-Independent Parameters for the Semi-analytical Chlorophyll Algorithm for Regions Without Packaged Pigments.

wavelength independent parameters							
X_0	−0.00182		S	0.0225		c_0	0.2818
X_1	2.058		p_0	51. 9		c_1	−2.783
Y_0	−1.13		p_1	1.00		c_2	1.863
Y_1	2.57					c_3	−2.387

Table 2. List of cruises with optical and bio-optical data collected by the University of South Florida (Carder data set) for initial tests of the unpackaged algorithm.

cruise	start date	end date	region	# stations
MLML 2	13 Aug 91	29 Aug 91	North Atlantic, 42EN–60EN	7
TT010	20 Jul 92	02 Aug 92	North Pacific, 24EN–48EN	10
GOMEX	10 Apr 93	19 Apr 93	Northern Gulf of Mexico	21
COLOR	31 May 93	09 Jun 93	Northern Gulf of Mexico	13
TN042	29 Nov 94	18 Dec 94	Arabian Sea	12
TN048	21 Jun 95	13 Jul 95	Arabian Sea	41

Total number of stations is 104

Table 3. Algorithm parameters used with the "packaged" and modified global data sets. All algorithm parameters not listed here are the same as in Table 1.

parameter	packaged	global
$a_0(412)$	1.90	1.95
$a_0(443)$	2.70	2.95
$a_0(488)$	1.90	1.99
$a_2(\lambda)$	-0.45	-0.5
$a_3(\lambda)$	0.021	0.025
p_0	74.1	72.4
p_1	1.0	1.0
c_0	0.4818	0.3147
c_1	−2.783	−2.859
c_2	1.863	2.007
c_3	−2.387	−1.730

Table 4. Summary of regression statistics for each data set tested. The unpackaged data consists of the Carder, EqPac above-surface, EqPac below-surface, Taiwan, and MOCE3 data sets. The packaged data consists of the CalCOFI and CAL9704 data sets. The global data consists of the global evaluation data set, minus the Cota and U. Maryland data plus the high-chlorophyll Carder, EqPac above-surface, Taiwan, and MOCE3 data, and uses one set of average algorithm parameters for the whole data set. SA indicates that only the modeled values that passed the semi-analytical portion of the algorithm are used (including blended values). SA+EMP indicates that all modeled values—semi-analytical, blended, and empirical—are used. All statistics except RMS2 are calculated from $\log_{10}$-transformed variables.

data set	variable	n	intercept	slope	bias	R^2	RMS1	RMS2
Carder	chl SA	86	0.019	1.020	0.010	0.921	0.122	0.289
Carder	chl SA+EMP	104	−0.007	0.977	−0.002	0.963	0.132	0.300
Carder	$a_\varphi(675)$ SA	82	0.098	1.052	−0.008	0.898	0.131	0.302
Carder	$a_g(400)$ SA	26	−0.278	0.905	−0.186	0.751	0.252	0.405
unpackaged	chl SA	261	0.001	0.999	0.002	0.873	0.099	0.230
unpackaged	chl SA+EMP	278	-0.019	0.973	-0.003	0.955	0.108	0.242
packaged	chl SA	303	-0.006	0.999	-0.006	0.917	0.111	0.268
packaged	chl SA+EMP	326	0.004	1.012	-0.003	0.951	0.114	0.282
global	chl SA	883	0.002	1.003	0.002	0.852	0.176	0.446
global	chl SA+EMP	976	0.003	1.003	0.002	0.913	0.174	0.440

Table 5. A list of cruises with optical and bio-optical data collected from southern and northern high latitude regions. When multiple R_{rs} and [chl a] values were available for the same date and time, the average value was used. 'n' is the number of stations with both R_{rs} and [chl a] data available. ACPZ is the Antarctic Polar Frontal Zone.

Cruise	P. Investigator	Institution	Dates	Location	n
ROAVERRS97	Arrigo, K	NASA/GSFC	12/97-1/98	Ross Sea	32
NBP9711	Mitchell, G.	UCSD/SIO	11/97-12/97	Ross Sea	20
REV9801	Mitchell, G.	UCSD/SIO	1/98	APFZ	9
REV9802	Mitchell, G.	UCSD/SIO	2/98	APFZ	2
AMLR2000	Mitchell, G.	UCSD/SIO	2/00-3/00	N. of Ant. Peninsula	21
AMLR2001	Mitchell, G.	UCSD/SIO	2/01-3/01	N. of Ant. Peninsula	29
LTER	Smith, R.	UCSB	1991-1999	W. of Ant. Peninsula	758
MF0796	Carder, K.	USF	4/96	Bering Sea	29
Ber96	Cota, G.	ODU	7/96	Bering Sea	6
Lab96	Cota, G.	ODU	10/96-11/96	Labrador Sea	2
Lab97	Cota, G.	ODU	5/97-6/97	Labador Sea	26
Lab00	Cota, G.	ODU	5/00-6/00	Labrador Sea	8
Goa97	Cota, G.	ODU	10/97	Gulf of Alaska	4

Table 6. Semi-analytical algorithm parameters for unpackaged and fully packaged data sets.

Parameter	Unpackaged	Fully packaged
$a_0(412)$	2.20	1.02
$a_0(443)$	3.59	1.89
$a_0(488)$	2.27	1.24
$a_0(510)$	1.40	0.84
$a_0(551)$	0.42	0.32
$a_1(412)$	0.75	0.26
$a_1(443)$	0.80	0.45
$a_1(488)$	0.59	0.42
$a_1(510)$	0.35	0.36
$a_1(551)$	-0.22	-0.08
$a_2(\lambda)$	-0.50	-0.45
$a_3(\lambda)$	0.0112	0.0210
p_0	51.9	79.4
p_1	1.0	1.0
c_0	0.2818	0.51
c_1	-2.783	-2.34
c_2	1.8630	0.40
c_3	-2.3870	0.00
S	0.0225	0.0170[*]
X_0	-0.00182	-0.00182
X_1	2.058	2.058
Y_0	-1.13	-1.13
Y_1	2.57	2.57

[*] A CDOM slope coefficient, S, of 0.0170 is used for Antarctic fully packaged data only. The slope for Arctic fully-packaged data shall remain 0.0225.

Table 7. Summary of regression statistics for each data set tested. The Antarctic data set consists of the following cruises: ROAVERRS97, NBP9711, REV9801, REV9802, AMLR2000, AMLR2001, and LTER. The Arctic data set includes cruises in the Bering Sea (MF0796 and Ber96), the Labrador Sea (Lab96, Lab97, + Lab00), and the Gulf of Alaska (Goa97). All statistics except RMS2 are calculated from $\log_{10}$-transformed variables.

Data Set	algorithm	n	Intercept	Slope	Bias	r^2	RMS1	RMS2	RMS_{lin}
Antarctic	Carder semi-analytic	871	-0.037	1.008	-0.036	0.82	0.219	0.718	0.525
Antarctic	SeaWiFS OC4v4	871	-0.271	1.022	-0.267	0.81	0.348	0.604	0.889
Arctic	Carder semi-analytic	75	-0.000	1.038	-0.009	0.82	0.172	0.465	0.406
Arctic	SeaWiFS OC4v4	75	-0.151	1.038	-0.143	0.83	0.223	0.398	0.537